J. Fluid Mech. (2013), *vol.* 736, *pp.* 464–494. © Cambridge University Press 2013
doi:10.1017/jfm.2013.549

Rayleigh–Bénard instability generated by a diffusion flame

P. Pearce and J. Daou†

School of Mathematics, University of Manchester, Manchester M13 9PL, UK

(Received 31 January 2013; revised 12 September 2013; accepted 14 October 2013;
first published online 8 November 2013)

We investigate the Rayleigh–Bénard convection problem within the context of a diffusion flame formed in a horizontal channel where the fuel and oxidizer concentrations are prescribed at the porous walls. This problem seems to have received no attention in the literature. When formulated in the low-Mach-number approximation the model depends on two main non-dimensional parameters, the Rayleigh number and the Damköhler number, which govern gravitational strength and reaction speed respectively. In the steady state the system admits a planar diffusion flame solution; the aim is to find the critical Rayleigh number at which this solution becomes unstable to infinitesimal perturbations. In the Boussinesq approximation, a linear stability analysis reduces the system to a matrix equation with a solution comparable to that of the well-studied non-reactive case of Rayleigh–Bénard convection with a hot lower boundary. The planar Burke–Schumann diffusion flame, which has been previously considered unconditionally stable in studies disregarding gravity, is shown to become unstable when the Rayleigh number exceeds a critical value. A numerical treatment is performed to test the effects of compressibility and finite chemistry on the stability of the system. For weak values of the thermal expansion coefficient α, the numerical results show strong agreement with those of the linear stability analysis. It is found that as α increases to a more realistic value the system becomes considerably more stable, and also exhibits hysteresis at the onset of instability. Finally, a reduction in the Damköhler number is found to decrease the stability of the system.

Key words: buoyancy-driven instability, combustion, flames

1. Introduction

The presence of flames in chemically reacting systems, whether premixed or non-premixed, naturally generates temperature gradients. Such systems are therefore prone to buoyancy-driven instabilities which have a paradigm in Rayleigh–Bénard convection. In this paper we revisit the Rayleigh–Bénard problem in the specific context of a diffusion or non-premixed flame, a fundamental problem which seems to have received no attention in the literature. The aim of the work is to complement the available knowledge on flame stability by determining the critical conditions which define the threshold of instability of a planar diffusion flame under gravitational effects.

The Rayleigh–Bénard problem itself has been important in work on the stability of physical systems since the early studies at the beginning of the 20th century by Bénard (1900) and Rayleigh (1916) on the natural convection of a fluid layer heated

† Email address for correspondence: joel.daou@manchester.ac.uk

https://doi.org/10.1017/jfm.2013.549 Published online by Cambridge University Press

from below. The temperature gradient in the system causes the fluid at the bottom of the layer to be lighter than the fluid at the top, an arrangement which becomes unstable if the temperature gradient is strong enough. The instability is opposed by the viscous forces of the fluid. It was in Lord Rayleigh's seminal paper that it was first demonstrated that a non-dimensional parameter which later became known as the Rayleigh number must exceed a critical value in order for the aforementioned instability to manifest itself. This parameter was defined in terms of the gravitational acceleration g, the height of the fluid layer L, the temperature gradient $\hat{\beta}$, and the coefficients of thermal expansion $\hat{\alpha}$, thermal diffusivity κ and kinematic viscosity ν as

$$Ra = \frac{g\hat{\alpha}\hat{\beta}L^4}{\kappa\nu}. \tag{1.1}$$

If the Rayleigh number exceeds its critical value, which may be denoted Ra_c, the resulting instability resolves itself into a steady state of 'convection rolls', observed by Bénard in his original experiments as a regular structure of hexagonal cells. The problem of determining the critical Rayleigh number and characterizing the resulting instabilities has been studied experimentally, numerically and analytically in a huge amount of research, which we do not review here. For a complete overview of the canonical problem see Chandrasekhar (1961, pp. 1–75) and literature reviews by Getling (1998, pp. 1–26) and Bodenschatz, Pesch & Ahlers (2000); more recent reviews concerning turbulence in Rayleigh–Bénard convection have been performed by Ahlers, Grossmann & Lohse (2009) and Lohse & Xia (2010).

The stability of steady states has also formed a crucial aspect of the study of both premixed and non-premixed flames. A thorough review of recent literature concerning flame instabilities has been performed by Matalon (2009). A further review concentrating on instabilities in premixed flames can be found in Bychkov *et al.* (2007); here we concentrate on instabilities in non-premixed combustion.

There have been a large number of studies on the diffusive-thermal instability of planar diffusion flames. Early studies focused on oscillatory instabilities of diffusion flames for fuel and oxidizer Lewis numbers greater than 1 (Kirkbey & Schmitz 1966; Cheatham & Matalon 1996*a*,*b*) before further studies including cellular instabilities for values of the Lewis number below 1 (Kim, Williams & Ronney 1996; Kim 1997; Cheatham & Matalon 2000; Kukuck & Matalon 2001; Vance, Miklavcic & Wichman 2001; Miklavčič, Moore & Wichman 2005; Metzener & Matalon 2006). The common factor in these studies is the use of the 'constant density approximation' which simplifies the study of combustion phenomena by separating the hydrodynamics from the equations for temperature and mass fractions. Recently this approximation was dispensed with by Matalon & Metzener (2010) to investigate the effect of thermal expansion on the stability of diffusion flames, again using the planar diffusion flame as the unperturbed state. It was found that, although thermal expansion does not play as crucial a role as it does for premixed flames, it influences the regions of parameter space for which the diffusive-thermal instability occurs.

A key point in the stability analyses previously performed on the planar diffusion flame in the absence of gravity is that of the unconditional stability of the Burke–Schumann diffusion flame, which arises in the limit of infinite reaction rate. Our study is motivated by the idea that the mechanism for the Rayleigh–Bénard instability described above could be expected to have a similar effect on a layer of fluid heated from below by a horizontal diffusion flame if buoyancy is taken into account, leading to instabilities of a system previously considered unconditionally

https://doi.org/10.1017/jfm.2013.549 Published online by Cambridge University Press

stable. There seems to our knowledge to be very little work addressing the effect of gravity on planar diffusion flames in the literature. Stability studies that have taken gravity into account have been focused on the flickering motion of diffusion flames (Buckmaster & Peters 1988; Arai, Sato & Amagai 1999; Jiang & Luo 2000), diffusion flames over a solid fuel (Wu & Chen 2003) or triple flames aligned with the gravity vector (Echekki, Chen & Hegde 2004).

In the present study we consider the stability of a horizontal planar diffusion flame in an infinitely long channel of given height under the effects of gravity. The main aim is to find the critical conditions for instability in the form of the critical value of a suitably defined Rayleigh number which defines the threshold of instability. An investigation into the instabilities in this problem will provide a crucial step towards a full understanding of the interaction between diffusion flames and hydrodynamics. Further areas that could benefit include studies into triple flames (which leave a trailing diffusion flame behind them) under gravitational effects.

We formulate the problem in the low-Mach-number approximation to filter out acoustic instabilities; a derivation of this formulation in the context of combustion was presented by Rehm & Baum (1978) and Majda & Sethian (1985). Further, in order to treat the problem analytically as far as possible we employ the Boussinesq approximation commonly used to study non-reactive Rayleigh–Bénard convection, which was derived by Boussinesq (1903). A rigorous derivation of this model from the general equations of combustion theory has been performed by Matkowsky & Sivashinsky (1979). The results of a linear stability analysis in this formulation can be compared to a numerical treatment of the non-Boussinesq equations in order to test the effect of compressibility on the system.

The paper is structured as follows. We begin in § 2 with a dimensional formulation of the low-Mach-number model, which we then non-dimensionalize and simplify in the Boussinesq approximation. We proceed in § 3 with an asymptotic analysis in the Burke–Schumann limit of infinite Damköhler number, followed by a linear stability analysis in § 4 using the planar Burke–Schumann flame as the base state. In § 5 we solve the linear stability problem for the growth rate eigenvalue numerically and analytically as far as possible to investigate the Rayleigh number at which the planar Burke–Schumann flame becomes unstable. In § 6 we present the results of the linear stability analysis, including how the critical Rayleigh number depends on the position of the flame in the channel. Finally, we compare these results in § 7 with a full numerical treatment to investigate the accuracy of the Boussinesq approximation and the effects of compressibility upon the stability of the system, followed by a short investigation of the effect of finite chemistry. The paper is closed with a discussion of the main findings and recommendations for future related studies.

2. Formulation

We investigate the problem of the stability of a planar diffusion flame in an infinitely long channel of height L. The channel walls are assumed to be porous with the fuel being provided at the upper wall and the oxidizer provided at the lower wall (see figure 1); for simplicity, the temperatures of the walls are assumed to be equal. Although this setup may be difficult to achieve experimentally, it is adopted here as a simple theoretical model to aid understanding of the effect of gravity on the planar diffusion flame. A similar setup has been used in several previous theoretical investigations (see e.g. Sohn, Chung & Kim 1999; Buckmaster & Jackson 2000; Daou & Al-Malki 2010). Since we are taking the effects of density changes and gravity into

https://doi.org/10.1017/jfm.2013.549 Published online by Cambridge University Press

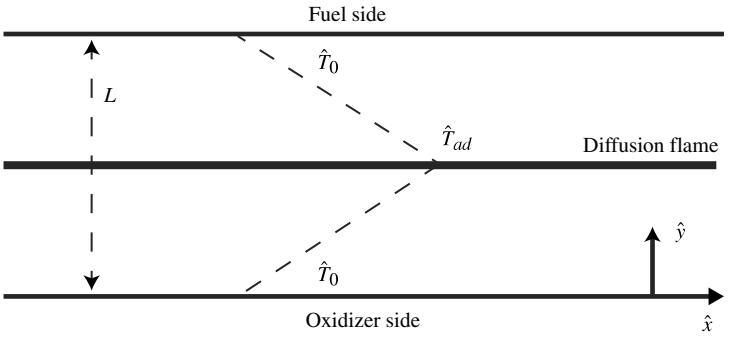


FIGURE 1. An illustration of a planar diffusion flame in a channel of height L with the fuel provided at the upper wall where $\hat{Y}_F = \hat{Y}_{F0}$, $\hat{Y}_O = 0$ and the oxidizer provided at the lower wall where $\hat{Y}_F = 0$, $\hat{Y}_O = \hat{Y}_{O0}$. Both walls are assumed to be rigid and to have equal temperatures $\hat{T} = \hat{T}_0$.

account, the governing equations will consist of the Navier–Stokes equations, coupled to equations for temperature and mass fractions of fuel and oxidizer. The combustion is modelled as a single irreversible one-step reaction of the form

$$F + sO \rightarrow (1+s)\text{Products} + q, \tag{2.1}$$

where F denotes the fuel and O the oxidizer. The quantity s denotes the mass of oxidizer consumed and q the heat released, both per unit mass of fuel.

The overall reaction rate $\hat{\omega}$ is taken to follow an Arrhenius law of the form

$$\hat{\omega} = \hat{\rho} B \hat{Y}_F \hat{Y}_O \exp(-E/R\hat{T}). \tag{2.2}$$

Here $\hat{\rho}$, $\hat{Y}_F$, $\hat{Y}_O$, R, $\hat{T}$, B and E are the density, the fuel mass fraction, the oxidizer mass fraction, the universal gas constant, the temperature, the pre-exponential factor and the activation energy of the reaction, respectively.

2.1. *Governing equations and boundary conditions*

To formulate the problem we adopt the low-Mach-number, common in flame theory and more rigorously justified using asymptotic analyses in several studies, such as those by Rehm & Baum (1978) and Majda & Sethian (1985). Under this approximation, the governing equations are

$$\frac{\partial \hat{\rho}}{\partial \hat{t}} + \boldsymbol{\nabla} \cdot \left(\hat{\rho}\hat{\boldsymbol{u}}\right) = 0, \tag{2.3}$$

$$\hat{\rho}\frac{\partial \hat{\boldsymbol{u}}}{\partial \hat{t}} + \hat{\rho}\hat{\boldsymbol{u}} \cdot \boldsymbol{\nabla}\hat{\boldsymbol{u}} + \boldsymbol{\nabla}\hat{P} = \mu\left(\nabla^2\hat{\boldsymbol{u}} + \tfrac{1}{3}\boldsymbol{\nabla}\left(\boldsymbol{\nabla} \cdot \hat{\boldsymbol{u}}\right)\right) + \hat{\rho}\hat{\boldsymbol{g}}, \tag{2.4}$$

$$\hat{\rho}\frac{\partial \hat{T}}{\partial \hat{t}} + \hat{\rho}\hat{\boldsymbol{u}} \cdot \boldsymbol{\nabla}\hat{T} - \frac{\partial \hat{P}}{\partial \hat{t}} = \hat{\rho} D_T \nabla^2 \hat{T} + \frac{q}{c_P}\hat{\omega}, \tag{2.5}$$

$$\hat{\rho}\frac{\partial \hat{Y}_F}{\partial \hat{t}} + \hat{\rho}\hat{\boldsymbol{u}} \cdot \boldsymbol{\nabla}\hat{Y}_F = \hat{\rho} D_F \nabla^2 \hat{Y}_F - \hat{\omega}, \tag{2.6}$$

$$\hat{\rho}\frac{\partial \hat{Y}_O}{\partial \hat{t}} + \hat{\rho}\hat{\boldsymbol{u}} \cdot \boldsymbol{\nabla}\hat{Y}_O = \hat{\rho} D_O \nabla^2 \hat{Y}_O - s\hat{\omega}, \tag{2.7}$$

$$\hat{P} = \hat{\rho} R \hat{T}, \tag{2.8}$$

https://doi.org/10.1017/jfm.2013.549 Published online by Cambridge University Press

where $\hat{}$ denotes dimensional terms and D_T, D_F, and D_O denote the diffusion coefficients of heat, fuel and oxidizer respectively. Here $\hat{\rho}D_T$, $\hat{\rho}D_F$ and $\hat{\rho}D_O$ are all assumed constant, as are the specific heat capacity c_P, thermal conductivity λ and dynamic viscosity μ.

As shown in figure 1 the walls are assumed to be rigid, porous and at the same temperature, giving the boundary conditions

$$\hat{T} = \hat{T}_0, \quad \hat{Y}_F = 0, \quad \hat{Y}_O = \hat{Y}_{O0}, \quad \hat{u} = \hat{v} = 0, \quad \text{at } \hat{y} = 0, \tag{2.9}$$

$$\hat{T} = \hat{T}_0, \quad \hat{Y}_F = \hat{Y}_{F0}, \quad \hat{Y}_O = 0, \quad \hat{u} = \hat{v} = 0, \quad \text{at } \hat{y} = L. \tag{2.10}$$

Owing to the assumption of low Mach number, the spatial variations in pressure are small. The total pressure can therefore be split into a background term consisting of thermodynamic pressure and a perturbational term consisting of hydrostatic pressure and hydrodynamic pressure (see Rehm & Baum 1978). We define the hydrodynamic pressure as

$$\hat{p}\left(\hat{\boldsymbol{x}}, \hat{t}\right) = \hat{P}\left(\hat{\boldsymbol{x}}, \hat{t}\right) - \hat{P}_0 - \hat{P}_s\left(\hat{\boldsymbol{x}}\right), \tag{2.11}$$

where $\hat{P}_0$ is the thermodynamic pressure, which we assume to be constant (see Buckmaster & Ludford 1983, p. 14) and given by the equation of state (2.8) as

$$\hat{P}_0 = \hat{\rho}_0 R \hat{T}_0. \tag{2.12}$$

Here $\hat{\rho}_0$ is the density in the absence of combustion. $\hat{P}_s(\hat{\boldsymbol{x}})$ is the hydrostatic pressure which satisfies the equation

$$\boldsymbol{\nabla}\hat{P}_s = \hat{\rho}_0 \hat{\boldsymbol{g}}. \tag{2.13}$$

This is found by considering (2.4) in the frozen limit with no flow (i.e. in hydrostatic equilibrium) and noting that, following from (2.12), the ambient atmosphere in the absence of heating must be taken to have constant density $\hat{\rho}_0$. Subtracting (2.13) from (2.4) then gives

$$\hat{\rho}\frac{\partial \hat{\boldsymbol{u}}}{\partial \hat{t}} + \hat{\rho}\hat{\boldsymbol{u}} \cdot \boldsymbol{\nabla}\hat{\boldsymbol{u}} + \boldsymbol{\nabla}\hat{p} = \mu\left(\nabla^2\hat{\boldsymbol{u}} + \tfrac{1}{3}\boldsymbol{\nabla}\left(\boldsymbol{\nabla} \cdot \hat{\boldsymbol{u}}\right)\right) + \left(\hat{\rho} - \hat{\rho}_0\right)\hat{\boldsymbol{g}}. \tag{2.14}$$

Now, since

$$\frac{\hat{p}\left(\hat{\boldsymbol{x}}, \hat{t}\right) + \hat{P}_s\left(\hat{\boldsymbol{x}}\right)}{\hat{P}_0} = O(M^2), \tag{2.15}$$

where M is the Mach number (see Paillere *et al.* 2000), the perturbational pressure term can be neglected in the ideal gas equation (2.8), which can then be written $\hat{P}_0 = \hat{\rho}R\hat{T}$ or, after considering (2.12),

$$\hat{\rho}\hat{T} = \hat{\rho}_0\hat{T}_0. \tag{2.16}$$

Before continuing we note that (2.5)–(2.7) have a steady, one-dimensional solution with no flow which, for large activation energy E, as typically encountered in combustion, is very close to the frozen solution (with zero reaction rate $\hat{\omega}$) given by

$$\hat{T} = \hat{T}_0, \tag{2.17}$$

$$\hat{Y}_F = \hat{Y}_{F0}\frac{\hat{y}}{L}, \tag{2.18}$$

$$\hat{Y}_O = \hat{Y}_{O0}\left(1 - \frac{\hat{y}}{L}\right). \tag{2.19}$$

https://doi.org/10.1017/jfm.2013.549 Published online by Cambridge University Press

Equations (2.17)–(2.19) determine the location of the stoichiometric surface $\hat{y} = \hat{y}_{st}$, where $\hat{Y}_O = s\hat{Y}_F$, and the values of the mass fractions there in the absence of combustion as

$$\frac{\hat{y}_{st}}{L} = \frac{1}{1+S}, \quad \hat{Y}_{F,st} = \frac{\hat{Y}_{F0}}{1+S}, \quad \hat{Y}_{O,st} = \frac{S\hat{Y}_{O0}}{1+S}, \tag{2.20}$$

where $S \equiv s\hat{Y}_{F0}/\hat{Y}_{O0}$ is a normalized stoichiometric coefficient.

We now introduce the non-dimensional variables

$$\left.\begin{aligned} &x = \frac{\hat{x}}{L}, \quad y = \frac{\hat{y}}{L}, \quad u = \frac{\hat{u}}{D_T/L}, \quad v = \frac{\hat{v}}{D_T/L}, \\ &t = \frac{\hat{t}}{L^2/D_T}, \quad \theta = \frac{\hat{T}-\hat{T}_0}{\hat{T}_{ad}-\hat{T}_0}, \quad y_F = \frac{\hat{Y}_F}{\hat{Y}_{F,st}}, \\ &y_O = \frac{\hat{Y}_O}{\hat{Y}_{O,st}}, \quad p = \frac{\hat{p}}{\hat{p}_0}; \end{aligned}\right\} \tag{2.21}$$

note that p is the small variation in pressure with reference unit $\hat{p}_0 = (D_T/L)^2\hat{\rho}_0$. Here the reference length L is the height of the channel. $\hat{T}_{ad}$ is the adiabatic flame temperature given by $\hat{T}_{ad} = \hat{T}_0 + q\hat{Y}_{F,st}/c_P$. The non-dimensional governing equations are then

$$\frac{\partial \rho}{\partial t} + \boldsymbol{\nabla}\cdot(\rho\boldsymbol{u}) = 0, \tag{2.22}$$

$$\rho\frac{\partial \boldsymbol{u}}{\partial t} + \rho\boldsymbol{u}\cdot\boldsymbol{\nabla}\boldsymbol{u} + \boldsymbol{\nabla}P^* = Pr\nabla^2\boldsymbol{u} + \frac{PrRa}{\alpha}(\rho-1)\frac{\boldsymbol{g}}{|\boldsymbol{g}|}, \tag{2.23}$$

$$\rho\frac{\partial \theta}{\partial t} + \rho\boldsymbol{u}\cdot\boldsymbol{\nabla}\theta = \nabla^2\theta + Da\omega, \tag{2.24}$$

$$\rho\frac{\partial y_F}{\partial t} + \rho\boldsymbol{u}\cdot\boldsymbol{\nabla}y_F = \frac{1}{Le_F}\nabla^2 y_F - Da\omega, \tag{2.25}$$

$$\rho\frac{\partial y_O}{\partial t} + \rho\boldsymbol{u}\cdot\boldsymbol{\nabla}y_O = \frac{1}{Le_O}\nabla^2 y_O - Da\omega, \tag{2.26}$$

where α is the thermal expansion coefficient $\alpha = (\hat{T}_{ad}-\hat{T}_0)/\hat{T}_{ad}$. Note that P^* is a modified pressure given by $P^* = p - (Pr/3)(\boldsymbol{\nabla}\cdot\boldsymbol{u})$. The non-dimensional parameters are

$$\left.\begin{aligned} &Ra = \frac{g(\hat{T}_{ad}-\hat{T}_0)L^3}{\nu\hat{T}_{ad}D_T}, \quad Da = \frac{4L^2}{\beta^3 D_T}Le_F Le_O B\hat{Y}_{O,st}\exp(-E/R\hat{T}_{ad}), \\ &Pr = \frac{\mu c_P}{\lambda}, \quad Le_F = \frac{D_T}{D_F}, \quad Le_O = \frac{D_T}{D_O}, \end{aligned}\right\} \tag{2.27}$$

which are the Rayleigh number, the Damköhler number, the Prandtl number and the fuel and oxidizer Lewis numbers, respectively. Here, β is the Zeldovich number or non-dimensional activation energy defined as $\beta = E(\hat{T}_{ad}-\hat{T}_0)/R\hat{T}_{ad}^2$. It is worth mentioning that we have defined the Rayleigh number to be of the form $Ra = g\Delta TL^3/\nu T_r D_T$, where ΔT measures the temperature difference and T_r is a reference temperature taken here to be $\hat{T}_{ad}$. This form has been adopted previously in the literature, for example in Fröhlich, Laure & Peyret (1992), where the reference temperature was taken to be an average value.

https://doi.org/10.1017/jfm.2013.549 Published online by Cambridge University Press

The non-dimensional reaction rate is given by

$$\omega = \frac{\beta^3}{4Le_F Le_O}\rho y_F y_O \exp\left(\frac{\beta(\theta-1)}{1+\alpha(\theta-1)}\right) \tag{2.28}$$

and the ideal gas equation (2.16) takes the non-dimensional form

$$\rho = \left(1+\frac{\alpha}{1-\alpha}\theta\right)^{-1}. \tag{2.29}$$

Finally, (2.9)–(2.10) and (2.20) imply that the boundary conditions are

$$\theta = 0, \quad y_F = 0, \quad y_O = \frac{S+1}{S}, \quad u = v = 0, \quad \text{at } y = 0, \tag{2.30}$$

$$\theta = 0, \quad y_F = 1+S, \quad y_O = 0, \quad u = v = 0, \quad \text{at } y = 1. \tag{2.31}$$

The non-dimensional problem is now fully formulated and is given by (2.22)–(2.29) with boundary conditions (2.30) and (2.31). The non-dimensional parameters in this problem are α, β, Pr, Ra, Da, S, Le_F and Le_O.

2.2. *Mixture fraction formulation*

2.2.1. *Formulation*

We can simplify the problem by making the assumption that $Le_F = Le_O = 1$. In this case we note that, from (2.24)–(2.26) and the boundary conditions (2.30)–(2.31), the quantity

$$\Phi = y_F + Sy_O + (S+1)(\theta-1) \tag{2.32}$$

satisfies the equation

$$\rho\frac{\partial\Phi}{\partial t} + \rho\boldsymbol{u}\cdot\nabla\Phi = \nabla^2\Phi, \tag{2.33}$$

subject to the boundary conditions

$$\Phi = 0 \quad \text{at } y = 0 \text{ and } y = 1. \tag{2.34}$$

Clearly $\Phi = 0$ is a stationary solution of (2.33)–(2.34). This will be the only solution we retain, in view of the focus of our linear stability analysis on the base state with no flow and $\Phi = 0$. A justification for retaining only this solution is presented below.

For solutions that are periodic in x of period L, define the L^2 scalar product

$$\langle\Phi, \Psi\rangle = \int_{x=0}^{L}\int_{y=0}^{1}\Phi\Psi\,\mathrm{d}x\,\mathrm{d}y, \tag{2.35}$$

with $\|\Phi\|^2 = \langle\Phi, \Phi\rangle$. Then (2.33) leads to

$$\left\langle\rho\frac{\partial\Phi}{\partial t}, \Phi\right\rangle + \langle\rho\boldsymbol{u}\cdot\nabla\Phi, \Phi\rangle = \left\langle\nabla^2\Phi, \Phi\right\rangle. \tag{2.36}$$

Using integration by parts and (2.22), this can be written

$$\frac{1}{2}\frac{\mathrm{d}}{\mathrm{d}t}\langle\rho\Phi, \Phi\rangle = -\left(\|\Phi_x\|^2 + \|\Phi_y\|^2\right), \tag{2.37}$$

or, using the Poincaré inequality and the fact that $0 < \rho \leqslant 1$,

$$\frac{1}{2}\frac{\mathrm{d}}{\mathrm{d}t}\langle\rho\Phi, \Phi\rangle \leqslant -c^2\|\Phi\|^2 \leqslant -c^2\langle\rho\Phi, \Phi\rangle, \tag{2.38}$$

https://doi.org/10.1017/jfm.2013.549 Published online by Cambridge University Press

for some constant c. Hence,

$$\langle \rho\Phi, \Phi\rangle \leqslant \Phi_0 \exp(-2c^2 t), \tag{2.39}$$

where $\Phi_0 = \langle \rho\Phi, \Phi\rangle\ (t=0)$. We therefore conclude that

$$\lim_{t\to\infty} \Phi = 0, \tag{2.40}$$

which justifies retaining only the stationary solution $\Phi = 0$.

It follows on using (2.32) that

$$y_F + Sy_O + (S+1)\theta = S + 1. \tag{2.41}$$

We now observe, by adding (2.24) and (2.25), that the quantity $y_F + \theta$ satisfies the equation

$$\rho\frac{\partial\,(y_F+\theta)}{\partial t} + \rho\boldsymbol{u}\cdot\boldsymbol{\nabla}\,(y_F+\theta) = \nabla^2\,(y_F+\theta)\,, \tag{2.42}$$

subject to the boundary conditions

$$y_F + \theta = 0 \quad \text{at } y = 0, \tag{2.43}$$

$$y_F + \theta = 1 + S \quad \text{at } y = 1. \tag{2.44}$$

This suggests defining the 'mixture fraction' Z by

$$y_F + \theta = (1+S)Z, \tag{2.45}$$

which implies that

$$y_O + \theta = \frac{S+1}{S}(1-Z). \tag{2.46}$$

The governing equations (2.22)–(2.26) then become

$$\frac{\partial\rho}{\partial t} + \boldsymbol{\nabla}\cdot(\rho\boldsymbol{u}) = 0, \tag{2.47}$$

$$\rho\frac{\partial\boldsymbol{u}}{\partial t} + \rho\boldsymbol{u}\cdot\boldsymbol{\nabla}\boldsymbol{u} + \boldsymbol{\nabla}P^* = Pr\nabla^2\boldsymbol{u} + \frac{PrRa}{\alpha}\,(\rho-1)\,\frac{\boldsymbol{g}}{|\boldsymbol{g}|}, \tag{2.48}$$

$$\rho\frac{\partial\theta}{\partial t} + \rho\boldsymbol{u}\cdot\boldsymbol{\nabla}\theta = \nabla^2\theta + Da\omega, \tag{2.49}$$

$$\rho\frac{\partial Z}{\partial t} + \rho\boldsymbol{u}\cdot\boldsymbol{\nabla}Z = \nabla^2 Z, \tag{2.50}$$

where

$$\omega = \frac{\beta^3}{4}\rho\,((1+S)Z-\theta)\left(\frac{1+S}{S}(1-Z)-\theta\right)\exp\left(\frac{\beta(\theta-1)}{1+\alpha(\theta-1)}\right), \tag{2.51}$$

and ρ is given by (2.29). These equations are subject to the boundary conditions

$$\theta = 0, \quad Z = 0, \quad u = v = 0, \quad \text{at } y = 0, \tag{2.52}$$

$$\theta = 0, \quad Z = 1, \quad u = v = 0, \quad \text{at } y = 1. \tag{2.53}$$

2.2.2. *Stationary planar diffusion flame*

The problem defined by (2.47)–(2.53) admits a stationary planar solution with no flow given by $Z = y$. The temperature can then be determined, using (2.49), by the

https://doi.org/10.1017/jfm.2013.549 Published online by Cambridge University Press

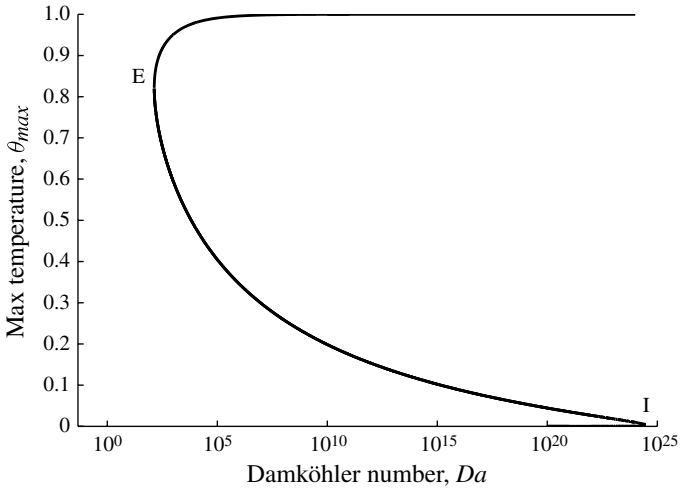


FIGURE 2. S-shaped curve generated by plotting the maximum temperature of the planar diffusion flame against the Damköhler number with labelled extinction (E) and ignition (I) points.

numerical solution to the equation

$$\frac{\mathrm{d}^2\theta}{\mathrm{d}y^2} + Da\frac{\beta^3}{4}\left(1+\frac{\alpha}{1-\alpha}\theta\right)^{-1}((1+S)y-\theta)\left(\frac{1+S}{S}(1-y)-\theta\right) \times \exp\left(\frac{\beta(\theta-1)}{1+\alpha(\theta-1)}\right) = 0, \tag{2.54}$$

with

$$\theta = 0 \quad \text{at } y = 0, \tag{2.55}$$

$$\theta = 0 \quad \text{at } y = 1. \tag{2.56}$$

Note that the Rayleigh number merely affects the pressure (as dictated by (2.48)) in the one-dimensional stationary system and does not affect the solution for temperature.

We now let β, α and S take typical values of 10, 0.85 and 1 respectively and solve (2.54) with conditions (2.55) and (2.56) for selected values of the Damköhler number Da. We use the boundary value problem solver BVP4C, a finite difference code that implements the three-stage Lobatto IIIa formula in Matlab (see Shampine, Kierzenka & Reichelt 2000). We then plot the maximum temperature of the solution against Da. Figure 2 shows the S-shaped curve that is generated; this is a classical curve characterizing diffusion flames and has been comprehensively studied in the context of the constant-density approximation (see Liñán 1974). The upper and lower branches are known as the strongly burning and weakly burning branches respectively, and both have been shown to be stable in the context of constant-density diffusion flames, while the middle branch has been shown to be unstable (see Buckmaster, Nachman & Taliaferro 1983).

Notable in figure 2 is the presence of an extinction and an ignition value of the Damköhler number represented by points E and I respectively; for values of Da below the extinction value the strongly burning solution cannot exist and for Da above the ignition value there is no weakly burning solution.

https://doi.org/10.1017/jfm.2013.549 Published online by Cambridge University Press

We are interested in instabilities caused by the effect of the hydrodynamics on the upper branch of the S-shaped curve, in particular in the Burke–Schumann limit of infinite Damköhler number. In § 7, we will numerically solve the governing equations in the mixture fraction formulation to investigate these instabilities; however, in order to treat the problem analytically as far as possible we now proceed with a reformulation of the problem in the Boussinesq approximation.

2.3. *Boussinesq approximation*

For a detailed derivation of the governing equations of combustion theory in the Boussinesq approximation in the context of a premixed flame see Sivashinsky (1977). Here we use a similar approach and assume that the thermal expansion parameter α is small. Thus we expand (2.29) as $\alpha \to 0$ to obtain

$$\rho = 1 - \alpha\theta + O\left(\alpha^2\right). \tag{2.57}$$

Using this result, and expanding all variables in successive powers of α in (2.47)–(2.53), yields to leading order

$$\boldsymbol{\nabla}\cdot\boldsymbol{u} = 0, \tag{2.58}$$

$$\frac{\partial \boldsymbol{u}}{\partial t} + \boldsymbol{u}\cdot\boldsymbol{\nabla}\boldsymbol{u} + \boldsymbol{\nabla}p = Pr\nabla^2\boldsymbol{u} - PrRa\theta\frac{\boldsymbol{g}}{|\boldsymbol{g}|}, \tag{2.59}$$

$$\frac{\partial\theta}{\partial t} + \boldsymbol{u}\cdot\boldsymbol{\nabla}\theta = \nabla^2\theta + Da\frac{\beta^3}{4}\left((1+S)Z-\theta\right)\left(\frac{1+S}{S}(1-Z)-\theta\right) \times \exp\left(\beta(\theta-1)\right), \tag{2.60}$$

$$\frac{\partial Z}{\partial t} + \boldsymbol{u}\cdot\boldsymbol{\nabla}Z = \nabla^2 Z, \tag{2.61}$$

which are subject to the boundary conditions (2.52)–(2.53).

We have thus reduced the number of equations in the unity-Lewis-number case so that the problem is now given by (2.58)–(2.61) with boundary conditions (2.52)–(2.53). We proceed with an asymptotic analysis of the problem in the infinitely fast chemistry limit $Da \to \infty$, which will reduce the problem to a form comparable to the classic non-reactive case studied by Chandrasekhar (1961) and others.

3. Asymptotic analysis

We now study the problem of the Burke–Schumann diffusion flame, which arises in the limit of infinite Damköhler number. In this case $y_F y_O = 0$ throughout the domain to prevent an unbounded reaction rate, except at an (infinitely thin) reaction sheet located at $y = y_{st}(t, x)$, say, where the temperature is equal to its adiabatic value. Hence, using (2.45)–(2.46),

$$y_F = (1+S)Z - \theta = 0, \quad y < y_{st}, \tag{3.1}$$

$$y_O = \frac{1+S}{S}(1-Z) - \theta = 0, \quad y > y_{st}, \tag{3.2}$$

$$\lim_{y\to y_{st}^{\pm}} \theta = 1. \tag{3.3}$$

Thus the domain is split into two parts: the region above the reaction sheet and the region below it, with

$$Z = \frac{1}{S+1}\theta, \quad y < y_{st}, \tag{3.4}$$

$$Z = 1 - \frac{S}{S+1}\theta, \quad y > y_{st}. \tag{3.5}$$

https://doi.org/10.1017/jfm.2013.549 Published online by Cambridge University Press

Note that (3.3) and (3.4)–(3.5) imply that

$$\lim_{y\to y_{st}^{\pm}} Z = \frac{1}{S+1} = Z_{st}, \tag{3.6}$$

which defines the stoichiometric mixture fraction Z_{st}.

We expand all variables outside the thin reaction zone, as $Da \to \infty$, in terms of the thickness of the reaction zone δ, where

$$\delta \sim Da^{-1/3} \ll 1. \tag{3.7}$$

This scaling follows from a reactive–diffusive balance in the reaction sheet. Indeed, writing $y_F \sim \delta y_F'$, $y_O \sim \delta y_O'$ and $\theta \sim 1 + \delta\theta'$ with $n = \delta n'$ inside the reaction sheet gives, from the leading order of (2.24),

$$\frac{\partial^2\theta'}{\partial n'^2} = Da\delta^3\omega', \tag{3.8}$$

where $\omega' = O(1)$. Thus, since the diffusion term and the reaction term (which are given by the left-hand side and the right-hand side of the equation above, respectively) must balance, we have the required scaling. We therefore write the outer expansions as

$$\left.\begin{aligned} \boldsymbol{u} &= \boldsymbol{u}^0 + \frac{\boldsymbol{u}^1}{Da^{1/3}} + \cdots, \quad p = p^0 + \frac{p^1}{Da^{1/3}} + \cdots, \\ \theta &= \theta^0 + \frac{\theta^1}{Da^{1/3}} + \cdots, \quad Z = Z^0 + \frac{Z^1}{Da^{1/3}} + \cdots. \end{aligned}\right\} \tag{3.9}$$

We now substitute into the governing equations (2.58)–(2.61) which become, to leading order

$$\frac{\partial u^0}{\partial x} + \frac{\partial v^0}{\partial y} = 0, \tag{3.10}$$

$$\frac{\partial u^0}{\partial t} + u^0\frac{\partial u^0}{\partial x} + v^0\frac{\partial u^0}{\partial y} + \frac{\partial p^0}{\partial x} = Pr\left(\frac{\partial^2 u^0}{\partial x^2} + \frac{\partial^2 u^0}{\partial y^2}\right), \tag{3.11}$$

$$\frac{\partial v^0}{\partial t} + u^0\frac{\partial v^0}{\partial x} + v^0\frac{\partial v^0}{\partial y} + \frac{\partial p^0}{\partial y} = Pr\left(\frac{\partial^2 v^0}{\partial x^2} + \frac{\partial^2 v^0}{\partial y^2}\right) + PrRa\theta^0, \tag{3.12}$$

$$\frac{\partial \theta^0}{\partial t} + u^0\frac{\partial \theta^0}{\partial x} + v^0\frac{\partial \theta^0}{\partial y} = \frac{\partial^2\theta^0}{\partial x^2} + \frac{\partial^2\theta^0}{\partial y^2}, \tag{3.13}$$

where we have

$$\theta^0 = (1+S)Z^0 \quad \text{for } y < y_{st} \quad \text{and} \quad \theta^0 = \frac{1+S}{S}\left(1 - Z^0\right) \text{ for } y > y_{st} \tag{3.14}$$

from (3.4)–(3.5), so that the equation for Z^0 is not necessary. These equations are subject to the boundary conditions

$$u^0 = v^0 = \theta^0 = 0 \quad \text{at } y = 0, \tag{3.15}$$

$$u^0 = v^0 = \theta^0 = 0 \quad \text{at } y = 1, \tag{3.16}$$

from (2.52)–(2.53). To close the problem we need to provide jump conditions across the reaction sheet located at $y = y_{st}(t, x)$. These are given by

$$\left[\theta^0\right] = \left[u^0\right] = \left[v^0\right] = 0, \tag{3.17}$$

https://doi.org/10.1017/jfm.2013.549 Published online by Cambridge University Press



FIGURE 3. A point P on the reaction sheet and its normal coordinate.

$$\left[\frac{\partial u^0}{\partial n}\right] = \left[p^0\right] - Pr\left[\frac{\partial v^0}{\partial n}\right] = 0, \tag{3.18}$$

$$\lim_{y\to y_{st}^{\pm}} \theta^0 = 1, \quad \frac{\partial \theta^0\left(y_{st}^-\right)}{\partial n} + S\frac{\partial \theta^0\left(y_{st}^+\right)}{\partial n} = 0, \tag{3.19}$$

where $[f] = f\left(y_{st}^+\right) - f\left(y_{st}^-\right)$ and n is a coordinate normal to the reaction sheet. A derivation of these in a general context has been presented by Cheatham & Matalon (2000), who assumed a large activation energy parameter $\beta \gg 1$, leading to leakages of the components through the reaction sheet. Since this is not the case here, for the convenience of the reader a short explanation of the derivation of conditions (3.17)–(3.19) is given in the remainder of this section, which can be skipped by those familiar with such an approach.

Consider a small neighbourhood of a point P on the reaction sheet, which has normal n as shown in figure 3. We temporarily consider a coordinate system with origin P and the y-axis directed along n. Thus in a small neighbourhood of P the reaction sheet is located at $y = 0$. We begin by assuming all state variables are continuous across the reaction sheet:

$$\left[\theta^0\right] = \left[Z^0\right] = 0, \tag{3.20}$$

with the notation $[f] = f\left(y = 0^+\right) - f\left(y = 0^-\right)$.

Now we introduce a stretched variable η given by

$$y = \frac{\eta}{Da^{1/3}} \tag{3.21}$$

and inner expansions in the thin reaction layer for all variables in terms of the thickness of the reaction sheet $\delta \sim Da^{-1/3}$,

$$\left.\begin{aligned} \boldsymbol{u} &= \boldsymbol{u}_0 + \frac{\boldsymbol{u}_1}{Da^{1/3}} + \cdots, \quad p = p_0 + \frac{p_1}{Da^{1/3}} + \cdots, \\ \theta &= \theta_0 + \frac{\theta_1}{Da^{1/3}} + \cdots, \quad Z = Z_0 + \frac{Z_1}{Da^{1/3}} + \cdots. \end{aligned}\right\} \tag{3.22}$$

Note that a subscript denotes successive terms in the inner expansion and a superscript denotes successive terms in the outer expansion of a variable. The inner and outer variables must satisfy matching conditions given by

$$\boldsymbol{u}_{inner}\left(\eta \to \pm\infty\right) = \boldsymbol{u}_{outer}\left(y \to 0^{\pm}\right), \tag{3.23}$$

for the velocity (and similar conditions on the other variables). Note that by expanding the outer solution around $y = 0$ we find

$$\boldsymbol{u}_0\left(\eta \to \pm\infty\right) = \boldsymbol{u}^0\left(y \to 0^{\pm}\right), \tag{3.24}$$

$$\boldsymbol{u}_1\left(\eta \to \pm\infty\right) = \eta\frac{\partial \boldsymbol{u}^0\left(y \to 0^{\pm}\right)}{\partial y} + \boldsymbol{u}^1\left(y \to 0^{\pm}\right) \tag{3.25}$$

https://doi.org/10.1017/jfm.2013.549 Published online by Cambridge University Press

for velocity (and similar conditions on the other variables). We substitute the inner variables into (2.58)–(2.61) and apply the matching conditions in order to derive jump conditions for the outer variables across the reaction sheet located at $y = 0$.

To leading order in (2.58)–(2.59), after substituting in the inner expansions (3.22), we find

$$\frac{\partial^2 u_0}{\partial \eta^2} = \frac{\partial v_0}{\partial \eta} = 0, \tag{3.26}$$

which can be integrated, using matching condition (3.24), to find

$$u_0 = \text{const}, \quad v_0 = \text{const}, \tag{3.27}$$

so that

$$\left[u^0\right] = \left[v^0\right] = 0. \tag{3.28}$$

At $O\left(Da^{1/3}\right)$ in the u momentum equation (2.59), after noting (3.27), we have

$$\frac{\partial^2 u_1}{\partial \eta^2} = 0. \tag{3.29}$$

Differentiating matching condition (3.25) with respect to η and applying to an integration of (3.29) then leads to

$$\left[\frac{\partial u^0}{\partial y}\right] = 0. \tag{3.30}$$

Similarly, we look to $O\left(Da^{1/3}\right)$ in the v momentum equation (2.59) and apply the differentiated form of matching condition (3.25) to find

$$\left[p^0\right] - Pr\left[\frac{\partial v^0}{\partial y}\right] = 0. \tag{3.31}$$

Since the temperature is adiabatic at the flame we already have condition (3.3) on the outer temperature profile, which gives

$$\lim_{y \to 0^{\pm}} \theta^0 = 1. \tag{3.32}$$

Finally, we have the jump condition on the mixture fraction, given by

$$\left[\frac{\partial Z^0}{\partial y}\right] = 0, \tag{3.33}$$

which is found by substituting (3.22) into (2.61) and integrating across the reaction sheet. From the relations (3.14) between θ^0 and Z^0, this gives the final condition

$$\frac{\partial \theta^0\left(y = 0^-\right)}{\partial y} + S\frac{\partial \theta^0\left(y = 0^+\right)}{\partial y} = 0. \tag{3.34}$$

The jump conditions above are valid at $y = 0$ in the coordinate system chosen. We can now generalize this to all points lying on the reaction sheet instead of just a neighbourhood of P (since P is arbitrary) and thus, by substitution of y with the normal coordinate n, the conditions at the reaction sheet are given by conditions (3.17)–(3.19) across $y = y_{st}$.

https://doi.org/10.1017/jfm.2013.549 Published online by Cambridge University Press

4. Linear stability analysis

Dropping the superscript notation from (3.10)–(3.14) gives the governing equations as

$$\frac{\partial u}{\partial x}+\frac{\partial v}{\partial y}=0, \tag{4.1}$$

$$\frac{\partial u}{\partial t}+u\frac{\partial u}{\partial x}+v\frac{\partial u}{\partial y}+\frac{\partial p}{\partial x}=Pr\left(\frac{\partial^2 u}{\partial x^2}+\frac{\partial^2 u}{\partial y^2}\right), \tag{4.2}$$

$$\frac{\partial v}{\partial t}+u\frac{\partial v}{\partial x}+v\frac{\partial v}{\partial y}+\frac{\partial p}{\partial y}=Pr\left(\frac{\partial^2 v}{\partial x^2}+\frac{\partial^2 v}{\partial y^2}\right)+PrRa\theta, \tag{4.3}$$

$$\frac{\partial \theta}{\partial t}+u\frac{\partial \theta}{\partial x}+v\frac{\partial \theta}{\partial y}=\frac{\partial^2 \theta}{\partial x^2}+\frac{\partial^2 \theta}{\partial y^2}, \tag{4.4}$$

$$\theta=(1+S)Z \text{ for } y<y_{st}, \quad \theta=\frac{1+S}{S}(1-Z) \text{ for } y>y_{st}. \tag{4.5}$$

These are to be solved on both sides of the reaction sheet located at $y=y_{st}$, with the boundary conditions

$$\theta=u=v=0 \quad \text{at } y=0, \tag{4.6}$$

$$\theta=u=v=0 \quad \text{at } y=1, \tag{4.7}$$

and the jump conditions

$$[\theta]=[u]=[v]=0, \tag{4.8}$$

$$\left[\frac{\partial u}{\partial n}\right]=[p]-Pr\left[\frac{\partial v}{\partial n}\right]=0, \tag{4.9}$$

$$\lim_{y\to y_{st}^{\pm}}\theta=1, \quad \frac{\partial\theta\left(y_{st}^{-}\right)}{\partial n}+S\frac{\partial\theta\left(y_{st}^{+}\right)}{\partial n}=0 \tag{4.10}$$

across $y=y_{st}$ (where n denotes a coordinate normal to the reaction sheet).

4.1. *Base state*

Equations (4.1)–(4.4) admit a stationary planar solution with no flow given by, using bars to denote the base state,

$$\frac{\mathrm{d}\bar{p}}{\mathrm{d}y}=PrRa\bar{\theta}, \quad \frac{\mathrm{d}^2\bar{\theta}}{\mathrm{d}y^2}=0, \tag{4.11}$$

subject to boundary conditions (4.6) and (4.7). Jump conditions (4.8)–(4.10) become

$$\left[\bar{\theta}\right]=[\bar{p}]=0, \tag{4.12}$$

$$\lim_{y\to \bar{y}_{st}^{\pm}}\bar{\theta}=1, \quad \frac{\mathrm{d}\bar{\theta}\left(\bar{y}_{st}^{-}\right)}{\mathrm{d}y}+S\frac{\mathrm{d}\bar{\theta}\left(\bar{y}_{st}^{+}\right)}{\mathrm{d}y}=0, \tag{4.13}$$

where $[f]=f\left(\bar{y}_{st}^{+}\right)-f\left(\bar{y}_{st}^{-}\right)$. It follows from (4.11)–(4.13) and conditions (4.6) and (4.7) that

$$\bar{\theta}=\frac{y}{\bar{y}_{st}}, \quad y<\bar{y}_{st}, \tag{4.14}$$

$$\bar{\theta}=\frac{1-y}{1-\bar{y}_{st}}, \quad y>\bar{y}_{st}. \tag{4.15}$$

https://doi.org/10.1017/jfm.2013.549 Published online by Cambridge University Press

Thus, using the condition on the right of (4.13),

$$\bar{y}_{st} = \frac{1}{1+S}, \tag{4.16}$$

so that

$$\bar{\theta} = (1+S)y, \quad y < \bar{y}_{st}, \tag{4.17}$$

$$\bar{\theta} = \frac{1+S}{S}(1-y), \quad y > \bar{y}_{st}. \tag{4.18}$$

Finally, the base-state pressure profile $\bar{p}$ can be found by integrating the equation on the left of (4.11) with respect to y.

4.2. *Linear stability problem*

We now perturb the base state by writing

$$u = \epsilon\tilde{u}, \quad v = \epsilon\tilde{v}, \quad p = \bar{p} + \epsilon\tilde{p}, \quad \theta = \bar{\theta} + \epsilon\tilde{\theta}, \quad y_{st} = \bar{y}_{st} + \epsilon\tilde{y}_{st}, \tag{4.19}$$

where $\epsilon \ll 1$ is a small parameter measuring the magnitude of the perturbations (denoted by tilde). To $O(\epsilon)$ in (4.1)–(4.4) we find

$$\frac{\partial\tilde{u}}{\partial x} + \frac{\partial\tilde{v}}{\partial y} = 0, \tag{4.20}$$

$$\frac{\partial\tilde{u}}{\partial t} + \frac{\partial\tilde{p}}{\partial x} = Pr\nabla^2\tilde{u}, \tag{4.21}$$

$$\frac{\partial\tilde{v}}{\partial t} + \frac{\partial\tilde{p}}{\partial y} = Pr\nabla^2\tilde{v} + PrRa\tilde{\theta}, \tag{4.22}$$

$$\frac{\partial\tilde{\theta}}{\partial t} + \tilde{v}\frac{\mathrm{d}\bar{\theta}}{\mathrm{d}y} = \nabla^2\tilde{\theta}. \tag{4.23}$$

The wall boundary conditions on the perturbed variables are given by, using (4.6)–(4.7),

$$\tilde{\theta} = \tilde{u} = \tilde{v} = 0 \quad \text{at } y = 0, \tag{4.24}$$

$$\tilde{\theta} = \tilde{u} = \tilde{v} = 0 \quad \text{at } y = 1. \tag{4.25}$$

Finally, we transfer the conditions (4.8)–(4.10) at the reaction sheet $y = y_{st}(t,x)$ to $y = \bar{y}_{st}$ by using a Taylor expansion around $y_{st} = \bar{y}_{st} + \epsilon\tilde{y}_{st}$. For example,

$$\theta(y_{st}) = \theta(\bar{y}_{st} + \epsilon\tilde{y}_{st}) = \theta(\bar{y}_{st}) + (y_{st} - \bar{y}_{st})\left(\theta_y(\bar{y}_{st})\right) + \cdots \tag{4.26}$$

which, using the perturbation to θ in (4.19), becomes

$$\theta(y_{st}) = \bar{\theta}(\bar{y}_{st}) + \epsilon\tilde{\theta}(\bar{y}_{st}) + \cdots + \epsilon\tilde{y}_{st}\bar{\theta}_y(\bar{y}_{st}) + \cdots \tag{4.27}$$

and therefore, at $O(\epsilon)$ of the condition to the left of (4.10),

$$\tilde{\theta} = -\tilde{y}_{st}\bar{\theta}_y \quad \text{at } y = \bar{y}_{st}^{\pm}. \tag{4.28}$$

Hence, using the base-state solution (4.17)–(4.18),

$$\tilde{\theta} = -\tilde{y}_{st}(1+S) \quad \text{at } y = \bar{y}_{st}^{-}, \tag{4.29}$$

$$\tilde{\theta} = \tilde{y}_{st}\frac{1+S}{S} \quad \text{at } y = \bar{y}_{st}^{+}. \tag{4.30}$$

https://doi.org/10.1017/jfm.2013.549 Published online by Cambridge University Press

The other reaction sheet conditions can be derived similarly, noting that u, v, their derivatives and p are continuous across the reaction sheet in the base state. This leads to

$$[\tilde{u}] = [\tilde{v}] = \left[\frac{\partial \tilde{u}}{\partial n}\right] = [\tilde{p}] - Pr\left[\frac{\partial \tilde{v}}{\partial n}\right] = 0 \quad \text{across } y = \bar{y}_{st}, \tag{4.31}$$

$$\left.\begin{aligned} &\tilde{\theta}\left(y = \bar{y}_{st}^{-}\right) = -\tilde{y}_{st}(1+S), \quad \tilde{\theta}\left(y = \bar{y}_{st}^{+}\right) = \tilde{y}_{st}\frac{1+S}{S}, \\ &S\tilde{\theta}_y\left(y = \bar{y}_{st}^{+}\right) + \tilde{\theta}_y\left(y = \bar{y}_{st}^{-}\right) = 0. \end{aligned}\right\} \tag{4.32}$$

The linear stability problem has now been derived and is given by (4.20)–(4.23) for $y \neq \bar{y}_{st}$, subject to the boundary conditions (4.24)–(4.25) and the jump conditions (4.31)–(4.32). It is worth noting that $\mathrm{d}\bar{\theta}/\mathrm{d}y$ takes different values below and above the reaction sheet, given by (4.17) and (4.18), respectively.

Before continuing, it can be noted that (4.20)–(4.23), which are four equations in four variables, can be simplified into two equations in two variables. To this end, we first take $(\partial/\partial x)$(4.21) + $(\partial/\partial y)$(4.22), which with the use of (4.20) gives

$$\nabla^2 \tilde{p} = PrRa\frac{\partial \tilde{\theta}}{\partial y}. \tag{4.33}$$

We then take ∇^2(4.22) to find

$$\frac{\partial}{\partial t}\nabla^2 \tilde{v} + \frac{\partial}{\partial y}\nabla^2 \tilde{p} = Pr\nabla^4 \tilde{v} + PrRa\nabla^2 \tilde{\theta}. \tag{4.34}$$

Finally, substitution of (4.33) into (4.34) yields

$$\frac{\partial}{\partial t}\nabla^2 \tilde{v} = Pr\nabla^4 \tilde{v} + PrRa\frac{\partial^2 \tilde{\theta}}{\partial x^2}. \tag{4.35}$$

Thus the perturbations $\tilde{v}$ and $\tilde{\theta}$ are governed by (4.23) and (4.35).

4.3. *Fourier analysis*

We consider normal-mode solutions by setting

$$\left.\begin{aligned} &\tilde{u} = U(y)\mathrm{e}^{\sigma t + \mathrm{i}ax}, \quad \tilde{v} = V(y)\mathrm{e}^{\sigma t + \mathrm{i}ax}, \quad \tilde{p} = \tilde{P}(y)\mathrm{e}^{\sigma t + \mathrm{i}ax}, \\ &\tilde{\theta} = \phi(y)\mathrm{e}^{\sigma t + \mathrm{i}ax}, \quad \tilde{y}_{st} = \mathrm{e}^{\sigma t + \mathrm{i}ax}. \end{aligned}\right\} \tag{4.36}$$

At this point it should be noted that three-dimensional perturbations of the form $\tilde{u} = U(y)\exp(\sigma t + \mathrm{i}(a_1 x + a_2 z))$, say, do not need to be considered because they lead to exactly the same problem, as derived below, if the substitution $a^2 = a_1^2 + a_2^2$ is made (known as Squire's transformation).

4.3.1. *Governing equations*

Note that for the derivation of the governing equations of the linear stability problem we do not need to consider $\tilde{u}$ or $\tilde{p}$, but we shall here nevertheless write the continuity equation and the momentum equations in terms of the Fourier variables, which follows from substituting (4.36) into (4.20)–(4.22), for future use:

$$\mathrm{i}aU + V' = 0, \tag{4.37}$$

$$\sigma U + \mathrm{i}a\tilde{P} = Pr(-a^2 U + U''), \tag{4.38}$$

$$\sigma V + \tilde{P}' = Pr(-a^2 V + V'') + PrRa\phi. \tag{4.39}$$

https://doi.org/10.1017/jfm.2013.549 Published online by Cambridge University Press

Continuing with the equations for $V(y)$ and $\phi(y)$, which follow from substituting (4.36) into (4.23) and (4.35), we have

$$\left(\mathrm{D}^2 - a^2 - \sigma\right)\phi = V\frac{\mathrm{d}\bar{\theta}}{\mathrm{d}y}, \tag{4.40}$$

$$\sigma\left(\mathrm{D}^2 - a^2\right)V = Pr\left(\mathrm{D}^2 - a^2\right)^2 V - a^2 PrRa\phi, \tag{4.41}$$

where $\mathrm{D} \equiv \mathrm{d}/\mathrm{d}y$.

Substitution of (4.40) into (4.41) gives a single equation for V in each region

$$\left(\mathrm{D}^2 - a^2 - \sigma\right)\left(\mathrm{D}^2 - a^2\right)\left(\mathrm{D}^2 - a^2 - \frac{\sigma}{Pr}\right)V = a^2 Ra\frac{\mathrm{d}\bar{\theta}}{\mathrm{d}y}V. \tag{4.42}$$

In other words, we have derived equations in the regions above and below the reaction sheet, which depend on the derivative of the base temperature in the respective region, given by (4.17) for $y < \bar{y}_{st}$ and (4.18) for $y > \bar{y}_{st}$.

Finally note that (4.41) implies that

$$\left(\mathrm{D}^2 - a^2\right)\left(\mathrm{D}^2 - a^2 - \frac{\sigma}{Pr}\right)V = a^2 Ra\phi, \tag{4.43}$$

which will be useful when deriving the boundary conditions in the next section.

4.3.2. *Boundary conditions*

On using (4.37) and (4.43), which give V in terms of U and ϕ respectively, boundary conditions (4.24)–(4.25) become, after substituting in (4.36),

$$V = \mathrm{D}V = \left(\mathrm{D}^2 - a^2\right)\left(\mathrm{D}^2 - a^2 - \frac{\sigma}{Pr}\right)V = 0 \quad \text{at } y = 0, 1. \tag{4.44}$$

4.3.3. *Jump conditions*

Conditions (4.32) can be written, after substituting in (4.36),

$$\phi\left(y = \bar{y}_{st}^-\right) = -(1+S), \quad \phi\left(y = \bar{y}_{st}^+\right) = \frac{1+S}{S}, \quad S\phi_y\left(y = \bar{y}_{st}^+\right) + \phi_y\left(y = \bar{y}_{st}^-\right) = 0. \tag{4.45}$$

The velocity jump conditions (4.31) convert to

$$[V] = [U] = [\mathrm{D}U] = 0 \quad \text{across } y = \bar{y}_{st}. \tag{4.46}$$

Also on using (4.31) we have

$$\left[\tilde{P}\right] = Pr\,[\mathrm{D}V] \quad \text{across } y = \bar{y}_{st}. \tag{4.47}$$

Now, considering (4.37) and its successive differentiations we can convert (4.46) to conditions on V, namely,

$$[V] = [\mathrm{D}V] = \left[\mathrm{D}^2 V\right] = 0 \quad \text{across } y = \bar{y}_{st}, \tag{4.48}$$

and thus, using (4.47),

$$\left[\tilde{P}\right] = 0 \quad \text{across } y = \bar{y}_{st}. \tag{4.49}$$

Finally, substitution of (4.37) into (4.38) gives

$$-a^2\tilde{P} = \sigma\mathrm{D}V + Pr\left(a^2 V - \mathrm{D}^3 V\right) \tag{4.50}$$

https://doi.org/10.1017/jfm.2013.549 Published online by Cambridge University Press

and hence (4.49) implies that

$$\left[\mathrm{D}^3 V\right] = 0 \quad \text{across } y = \bar{y}_{st}. \tag{4.51}$$

Thus the linear stability problem for the system is fully formulated. It is given by

$$\left(\mathrm{D}^2 - a^2 - \sigma\right)\left(\mathrm{D}^2 - a^2\right)\left(\mathrm{D}^2 - a^2 - \frac{\sigma}{Pr}\right) V = a^2 Ra(1+S)V, \quad y < \bar{y}_{st}, \tag{4.52}$$

$$\left(\mathrm{D}^2 - a^2 - \sigma\right)\left(\mathrm{D}^2 - a^2\right)\left(\mathrm{D}^2 - a^2 - \frac{\sigma}{Pr}\right) V = -a^2 Ra\frac{(1+S)}{S}V, \quad y > \bar{y}_{st}, \tag{4.53}$$

with the wall boundary conditions

$$V = \mathrm{D}V = \left(D^2 - a^2\right)\left(\mathrm{D}^2 - a^2 - \frac{\sigma}{Pr}\right) V = 0 \text{ at } y = 0, 1, \tag{4.54}$$

the mass/momentum jump conditions

$$[V] = [\mathrm{D}V] = [\mathrm{D}^2 V] = [\mathrm{D}^3 V] = 0 \quad \text{across } y = \bar{y}_{st} \tag{4.55}$$

and the reaction sheet conditions

$$\left(\mathrm{D}^2 - a^2\right)\left(\mathrm{D}^2 - a^2 - \frac{\sigma}{Pr}\right) V = -a^2 Ra(1+S) \quad \text{at } y = \bar{y}_{st}^-, \tag{4.56}$$

$$\left(\mathrm{D}^2 - a^2\right)\left(\mathrm{D}^2 - a^2 - \frac{\sigma}{Pr}\right) V = a^2 Ra\frac{1+S}{S} \quad \text{at } y = \bar{y}_{st}^+, \tag{4.57}$$

$$S\left(\mathrm{D}\left(\mathrm{D}^2 - a^2\right)\left(\mathrm{D}^2 - a^2 - \frac{\sigma}{Pr}\right) V\left(\bar{y}_{st}^+\right)\right) + \mathrm{D}\left(\mathrm{D}^2 - a^2\right)\left(\mathrm{D}^2 - a^2 - \frac{\sigma}{Pr}\right) V\left(\bar{y}_{st}^-\right) = 0, \tag{4.58}$$

where the averaged flame position is given by $\bar{y}_{st} = 1/(1+S)$.

We now have a sixth-order ordinary differential equation for the velocity perturbation V in each region, with 13 auxiliary conditions (six boundary conditions at the wall and seven conditions at the averaged reaction sheet). These conditions are sufficient to determine V along with the eigenvalue $\sigma = \sigma(a; Ra, S)$, which will determine the linear stability of the Burke–Schumann diffusion flame. For given values of Ra and S, if the real part of the growth rate σ is greater than zero for any value of the wavenumber a, the system is unstable. If the real part of σ is negative for all values of a the system is stable.

5. Solution of the linear stability problem

It is worth noting at this point that in the non-reactive case it can be shown that the growth rate σ is real and the marginal state is characterized by $\sigma = 0$; this is called the principle of the exchange of stabilities (see Chandrasekhar 1961, pp. 24–26). Since this is not straightforward in our case, we instead begin by solving the linear stability problem numerically using the BVP4C solver in Matlab to find the eigenvalue σ and investigate whether its imaginary part is zero at marginal stability. If so, we can characterize the marginal state as the state where $\sigma = 0$ and proceed to solve the problem in a similar approach to the non-reactive case.

5.1. *Numerical solution for* σ

In this section, we numerically solve (4.52) and (4.53) with conditions (4.54)–(4.58). We use the eigen-boundary-value-problem Matlab solver BVP4C (see Shampine *et al.*

https://doi.org/10.1017/jfm.2013.549 Published online by Cambridge University Press

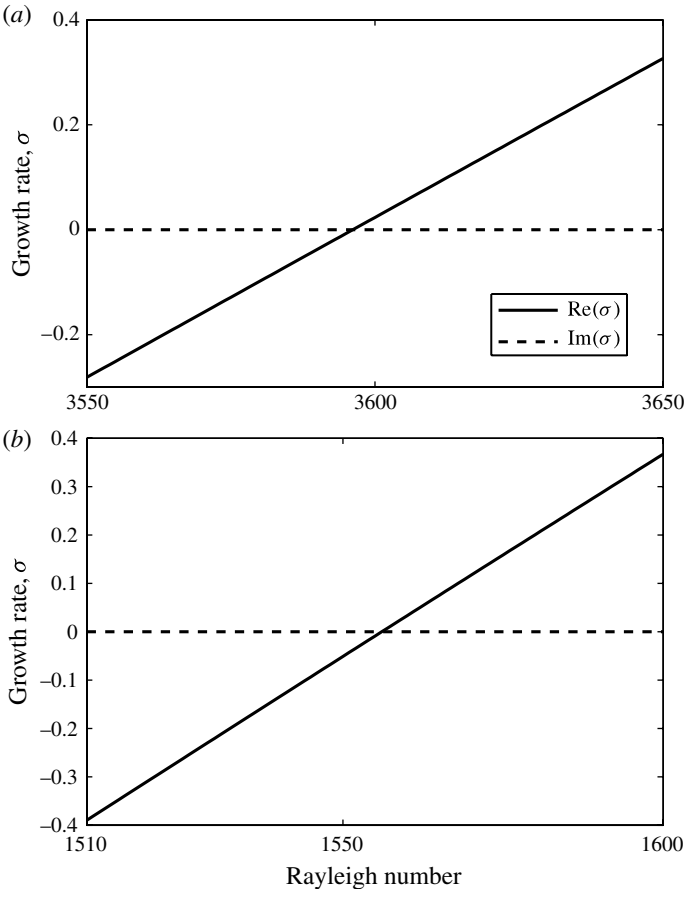


FIGURE 4. Graphs of real and imaginary parts of the growth rate σ versus the Rayleigh number Ra for two selected values of the stoichiometric coefficient S (with $Pr = 1$): (*a*) $S = 1$ with wavenumber $a = 3.95$; (*b*) $S = 5$ with wavenumber $a = 3.13$. Note that the imaginary part of the growth rate is found to be zero for all values of Ra.

2000) to find the value of the growth rate σ for given values of the wavenumber a, the Rayleigh number Ra and the stoichiometric coefficient S. The key result is that σ is always found to be real. Figure 4 shows that as Ra increases for selected values of a and S, σ passes from negative values to positive values and there is a marginal value of Ra at which the system changes from stability to instability and $\sigma = 0$. We also plot the effect of the wavenumber on the growth rate for several values of the Rayleigh number in figure 5, which clearly shows the existence of a critical Rayleigh number. If the Rayleigh number takes a value higher than its critical value, there is a band of wavenumbers for which $\sigma > 0$ and the system is unstable.

At this point we could produce many more plots investigating the stability of the system; however to avoid repetition we merely note that the growth rate is always found to be real and thus $\sigma = 0$ characterizes the marginal state. We can therefore simplify the problem by setting $\sigma = 0$ in the governing equations and then solve to find the marginal Rayleigh number. In the next section we will solve the marginal problem and then discuss the stability of the system in more detail.

https://doi.org/10.1017/jfm.2013.549 Published online by Cambridge University Press

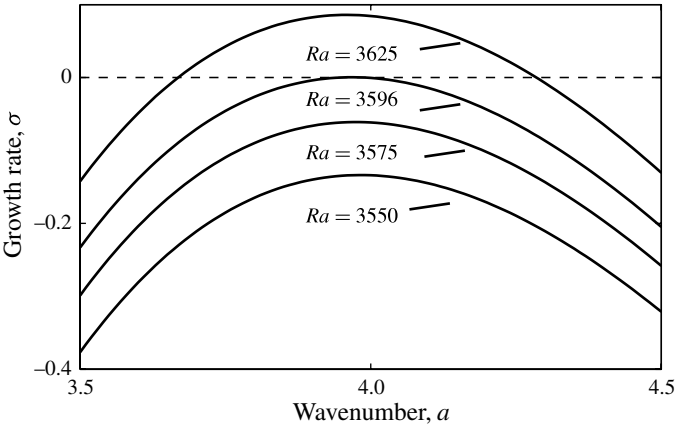


FIGURE 5. Growth rate versus wavenumber for selected values of the Rayleigh number, with $S = 1$ and $Pr = 1$. Note that in this case the critical Rayleigh number is found to be $Ra_c = 3596$.

5.2. *Marginal state*

Motivated by the conclusions of the previous section, here we set $\sigma = 0$ in (4.52) and (4.53) with conditions (4.54)–(4.58), characterizing the marginal state. This is the state at which the system passes from being stable to being unstable, and thus the Rayleigh number for which this state exists for a given wavenumber a is the marginal Rayleigh number at that wavenumber. Hence

$$\left(\mathrm{D}^2 - a^2\right)^3 V = a^2 Ra(1+S)V, \quad y < \bar{y}_{st}, \tag{5.1}$$

$$\left(\mathrm{D}^2 - a^2\right)^3 V = -a^2 Ra\frac{(1+S)}{S}V, \quad y > \bar{y}_{st}, \tag{5.2}$$

with the wall boundary conditions

$$V = \mathrm{D}V = \left(\mathrm{D}^2 - a^2\right)^2 V = 0 \quad \text{at } y = 0,\, 1, \tag{5.3}$$

the mass/momentum jump conditions

$$[V] = [\mathrm{D}V] = \left[\mathrm{D}^2 V\right] = \left[\mathrm{D}^3 V\right] = 0 \quad \text{across } y = \bar{y}_{st} \tag{5.4}$$

and the reaction sheet conditions

$$\left(\mathrm{D}^2 - a^2\right)^2 V = -a^2 Ra(1+S) \quad \text{at } y = \bar{y}_{st}^-, \tag{5.5}$$

$$\left(\mathrm{D}^2 - a^2\right)^2 V = a^2 Ra\frac{1+S}{S} \quad \text{at } y = \bar{y}_{st}^+, \tag{5.6}$$

$$S\left(\mathrm{D}\left(\mathrm{D}^2 - a^2\right)^2 V\left(\bar{y}_{st}^+\right)\right) + \mathrm{D}\left(\mathrm{D}^2 - a^2\right)^2 V\left(\bar{y}_{st}^-\right) = 0, \tag{5.7}$$

where the averaged flame position is given by $\bar{y}_{st} = 1/(1+S)$.

Following a similar approach to that of Chandrasekhar (1961, pp. 36–42), we let the velocity perturbation V take the form

$$V = \mathrm{e}^{\pm py}, \quad y < \bar{y}_{st}, \tag{5.8}$$

$$V = \mathrm{e}^{\pm qy}, \quad y > \bar{y}_{st}. \tag{5.9}$$

https://doi.org/10.1017/jfm.2013.549 Published online by Cambridge University Press

Then we have

$$\left(p^2 - a^2\right)^3 = a^2 Ra(1+S), \quad y < \bar{y}_{st}, \tag{5.10}$$

$$\left(q^2 - a^2\right)^3 = -a^2 Ra\frac{(1+S)}{S}, \quad y > \bar{y}_{st}. \tag{5.11}$$

If we let

$$\frac{1+S}{S}a^2 Ra = \tau^3 a^6 \tag{5.12}$$

we find that the roots of these equations are given by

$$p^2 = a^2\left(S^{1/3}\tau + 1\right) \quad \text{and} \quad p^2 = a^2\left[1 + S^{1/3}\frac{\tau}{2}\left(-1 \pm \mathrm{i}\sqrt{3}\right)\right], \tag{5.13}$$

$$q^2 = -a^2(\tau - 1) \quad \text{and} \quad q^2 = a^2\left[1 + \frac{\tau}{2}\left(1 \pm \mathrm{i}\sqrt{3}\right)\right]. \tag{5.14}$$

Thus we have six roots for the solution below the reaction sheet and six roots for the solution above it, given by

$$\pm p_0, \quad \pm p \quad \text{and} \quad \pm p^*, \tag{5.15}$$

$$\pm \mathrm{i}q_0, \quad \pm q \quad \text{and} \quad \pm q^*, \tag{5.16}$$

where * denotes the complex conjugate. Here

$$p_0 = a\sqrt{\left(S^{1/3}\tau + 1\right)}, \tag{5.17}$$

$$\mathrm{Re}(p) = a\left[\frac{1}{2}\left(\sqrt{1 - S^{1/3}\tau + S^{2/3}\tau^2} + \left(1 - S^{1/3}\frac{\tau}{2}\right)\right)\right]^{1/2}, \tag{5.18}$$

$$\mathrm{Im}(p) = a\left[\frac{1}{2}\left(\sqrt{1 - S^{1/3}\tau + S^{2/3}\tau^2} - \left(1 - S^{1/3}\frac{\tau}{2}\right)\right)\right]^{1/2}, \tag{5.19}$$

and

$$q_0 = a\sqrt{(\tau - 1)}, \tag{5.20}$$

$$\mathrm{Re}(q) = a\left[\frac{1}{2}\left(\sqrt{1 + \tau + \tau^2} + \left(1 + \frac{\tau}{2}\right)\right)\right]^{1/2}, \tag{5.21}$$

$$\mathrm{Im}(q) = a\left[\frac{1}{2}\left(\sqrt{1 + \tau + \tau^2} - \left(1 + \frac{\tau}{2}\right)\right)\right]^{1/2}. \tag{5.22}$$

Thus the solution for the velocity perturbation can be written as

$$V^- = A_0\cosh p_0 y + A\cosh py + A^*\cosh p^* y + B_0\sinh p_0 y + B\sinh py + B^*\sinh p^* y, \quad y < \bar{y}_{st}, \tag{5.23}$$

$$V^+ = C_0\cos q_0 y + C\cosh qy + C^*\cosh q^* y + D_0\sin q_0 y + D\sinh qy + D^*\sinh q^* y, \quad y > \bar{y}_{st}. \tag{5.24}$$

The problem has 13 auxiliary conditions while the general solution has 12 constants of integration. We therefore need to apply 12 conditions in order to determine $V^{\pm}$ for a specified value of a and use the 13th condition to determine τ, from which we can find the marginal Rayleigh number using the formula

$$Ra = \tau^3 a^4 \frac{S}{1+S}. \tag{5.25}$$

https://doi.org/10.1017/jfm.2013.549 Published online by Cambridge University Press

To write the boundary conditions on V in matrix form, we begin by noting, using (5.23)–(5.24), that

$$\begin{aligned}\left(\mathrm{D}^2-a^2\right)^2 V^- = S^{2/3}a^4\tau^2 \Big[&A_0\cosh p_0 y - \tfrac{1}{2}\left(\mathrm{i}\sqrt{3}+1\right)A\cosh py \\ &- \tfrac{1}{2}\left(-\mathrm{i}\sqrt{3}+1\right)A^*\cosh p^* y + B_0\sinh p_0 y \\ &- \tfrac{1}{2}\left(\mathrm{i}\sqrt{3}+1\right)B\sinh py - \tfrac{1}{2}\left(-\mathrm{i}\sqrt{3}+1\right)B^*\sinh p^* y\Big], \quad (5.26)\end{aligned}$$

and

$$\begin{aligned}\left(\mathrm{D}^2-a^2\right)^2 V^+ = a^4\tau^2 \Big[&C_0\cos q_0 y + \tfrac{1}{2}\left(\mathrm{i}\sqrt{3}-1\right)C\cosh qy \\ &- \tfrac{1}{2}\left(\mathrm{i}\sqrt{3}+1\right)C^*\cosh q^* y + D_0\sin q_0 y \\ &+ \tfrac{1}{2}\left(\mathrm{i}\sqrt{3}-1\right)D\sinh qy - \tfrac{1}{2}\left(\mathrm{i}\sqrt{3}+1\right)D^*\sinh q^* y\Big]. \quad (5.27)\end{aligned}$$

The conditions (5.3)–(5.6) can then be written in the matrix form $\boldsymbol{A}\boldsymbol{x}=\boldsymbol{b}$ for the vector of constants $\boldsymbol{x}$, which can be solved using

$$\boldsymbol{x}=\boldsymbol{A}^{-1}\boldsymbol{b}. \quad (5.28)$$

We then write the final condition (5.7), say, as

$$\boldsymbol{c}^T\boldsymbol{x}=0, \quad (5.29)$$

where $\boldsymbol{c}$ is a vector. A solution that satisfies all of the auxiliary conditions can therefore be found by solving the matrix (5.28) for given values of a and S in Matlab to find $\boldsymbol{x}$ and then using Matlab's fzero function with $\boldsymbol{c}^T\boldsymbol{x}$ as the input. This will lead to a solution for $V^{\pm}$ and τ, from which the marginal Rayleigh number can be found using (5.25). Note that the temperature perturbation profile can be recovered from the velocity perturbation profile using the equations

$$\phi^{\pm}=\frac{(1+S)}{S\tau^3a^6}\left(\mathrm{D}^2-a^2\right)V^{\pm}. \quad (5.30)$$

6. Discussion of results

In this section we present the results found by solving the problem in the marginal state using the method described at the end of the previous section. The aim is to calculate the critical Rayleigh number Ra_c, which characterizes the conditions at the threshold of instability, and its dependence upon the stoichiometric coefficient S.

We begin with plots of how the Rayleigh number in the marginal state varies with the wavenumber a for two selected values of the stoichiometric coefficient S, provided in figure 6. Indicated in the figure are the calculated values of the critical Rayleigh number Ra_c and the corresponding critical wavenumber a_c for each value of S. It can be seen that, for a given value of S, if $Ra > Ra_c$ there is a band of wavenumbers for which the growth rate $\sigma > 0$; thus if $Ra > Ra_c$ the perturbations made to the base state grow exponentially in time and the system is unstable. Velocity perturbation profiles versus y at the onset of instability $Ra = Ra_c$ for selected values of S are presented in figure 7.

Next we plot, in figure 8, the variation in Ra_c with the stoichiometric coefficient S and the flame position $y_{st} = 1/(1+S)$. Indicated in each plot is the critical Rayleigh

https://doi.org/10.1017/jfm.2013.549 Published online by Cambridge University Press

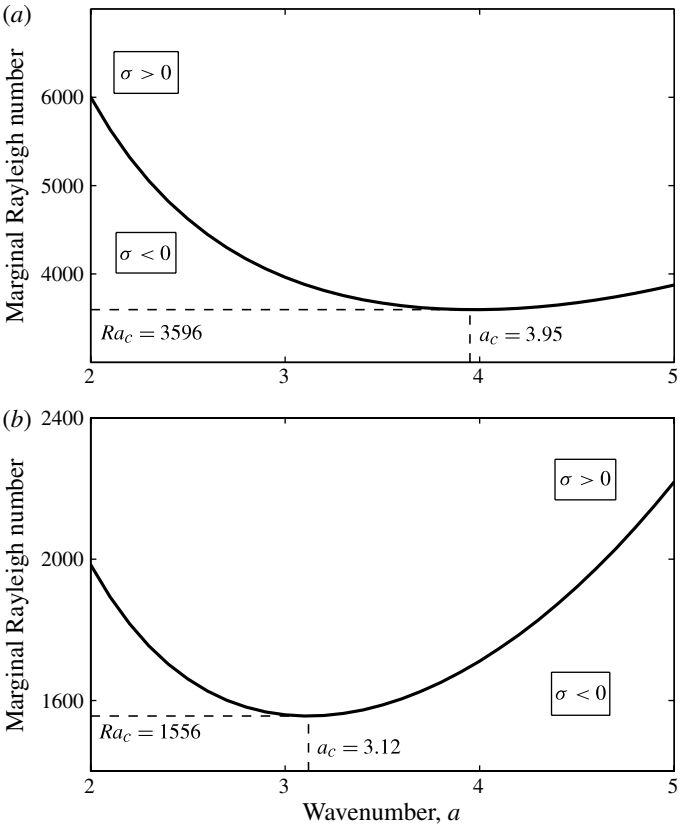


FIGURE 6. Marginal Rayleigh number versus wavenumber for two selected values of the stoichiometric coefficient: (*a*) $S = 1$; (*b*) $S = 5$. For each wavenumber the system is unstable if the Rayleigh number Ra takes a value larger than the marginal Rayleigh number, and stable if Ra is lower. For each value of S, the lowest marginal Rayleigh number is the critical Rayleigh number Ra_c and the corresponding wavenumber is the critical wavenumber a_c.

number given in Chandrasekhar (1961, p. 39) for the non-reactive problem with two rigid boundaries. The fact that Ra_c in our reactive case is found to be very close to the non-reactive critical Rayleigh number for large values of S, but not exactly equal in the limit $S \to \infty$, can be explained by considering the equations governing the marginal state. As $S \to \infty$, the problem in the upper half-space above the reaction sheet reduces to the non-reactive problem with two rigid boundaries, except for the conditions (5.5) and (5.6) at the reaction sheet. Thus, as $S \to \infty$ the critical Rayleigh number approaches a value slightly different to the non-reactive critical Rayleigh number, as can be seen in figure 8. It is found that as the flame moves away from the lower boundary, Ra_c first decreases slightly then increases to very large values as the flame approaches the upper boundary.

It can be seen in figure 8 that the order of magnitude of Ra_c can significantly deviate from the order of magnitude of the critical Rayleigh number in the non-reactive case, especially as $y_{st} \to 1$. In order to facilitate comparison with the non-reactive case, we scale the Rayleigh number, by using as reference length the distance of the flame from the upper boundary $(1 - y_{st})\,L$ instead of L. This scaled Rayleigh

https://doi.org/10.1017/jfm.2013.549 Published online by Cambridge University Press

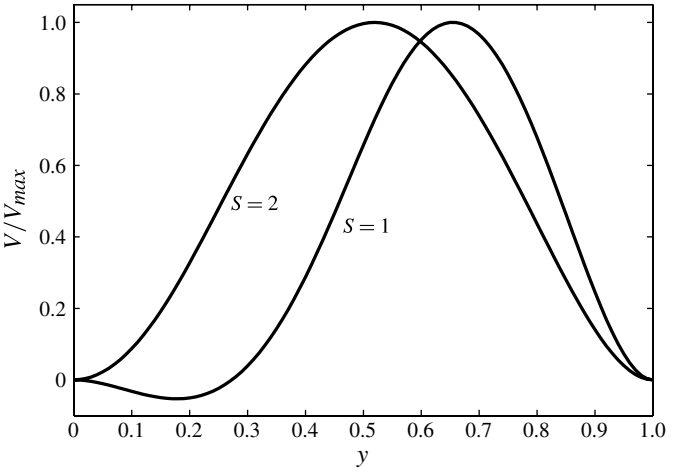


FIGURE 7. Marginal velocity perturbation profile $V^{\pm}$ versus y for two selected values of the stoichiometric coefficient S (scaled by the maximum value for comparison). In each case the wavenumber a is equal to its critical value a_c, given by $a_c = 3.95$ for $S = 1$ and $a_c = 3.25$ for $S = 2$.

number is more comparable to the Rayleigh number in the non-reactive case because both use as reference length the distance from the hot surface to the cold upper boundary. The scaled critical Rayleigh number is given by

$$Ra_{c,scaled} = Ra_c(1 - y_{st})^3. \tag{6.1}$$

In figure 9 we plot $Ra_{c,scaled}$ against the flame position y_{st} and the stoichiometric coefficient S and compare with two non-reactive cases. The first is the case of two rigid boundaries; the second is the case of one rigid boundary and one free-surface boundary. Similarly to above it is found that, as $S \to \infty$, $Ra_{c,scaled}$ is of the order of magnitude of the critical Rayleigh number in the rigid–rigid non-reactive case. It is also found that for $S \approx 9$ (i.e. $y_{st} \approx 0.1$), $Ra_{c,scaled}$ is of the order of magnitude of the critical Rayleigh number in the rigid–free non-reactive case. As the flame approaches the upper boundary, in the limit $S \to 0$, $Ra_{c,scaled}$ decreases to lower values.

7. Numerical study

We now proceed to a full numerical treatment of the problem, using the finite element package Comsol Multiphysics to directly simulate the physical system. We solve the time-dependent equations (2.47)–(2.51) with boundary conditions (2.52)–(2.53). As initial condition we use the strongly burning planar diffusion flame (which is found on the upper branch of the curve in figure 2). The aims in this section are: first, to investigate the nature of the instabilities that occur for values of the Rayleigh number slightly higher than Ra_c; secondly, to test the results of the linear stability analysis presented in the previous section against numerical results; finally, to test the effect of thermal expansion and finite chemistry on Ra_c.

All numerical calculations are performed for the parameter values $\beta = 10$ and $Pr = 1$, in a numerical domain of aspect ratio 10; this aspect ratio has been shown to be sufficiently large to approximate an infinite domain in the non-reactive case by Gelfgat (1999). The domain is discretized into a non-uniform grid of approximately

https://doi.org/10.1017/jfm.2013.549 Published online by Cambridge University Press

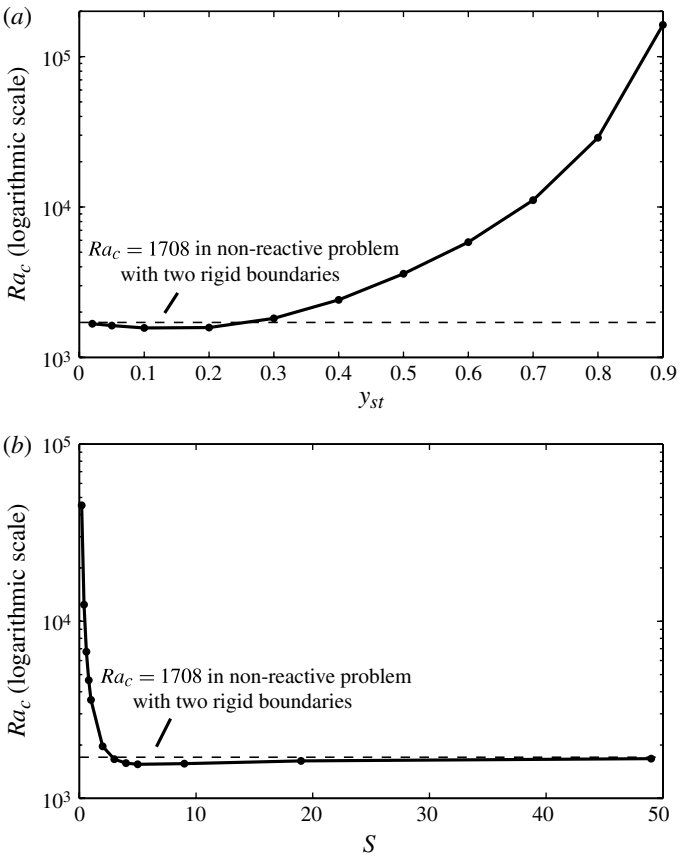


FIGURE 8. The effect of (*a*) the flame position $y_{st} = 1/(1 + S)$ and (*b*) the stoichiometric coefficient S on the critical Rayleigh number Ra_c. Indicated with a dashed line is the critical Rayleigh number in non-reactive Rayleigh–Bénard convection with two rigid boundaries.

120 000 triangular elements, with local refinement around the reaction zone and the upper and lower boundaries; various tests have been performed to ensure the mesh-independence of the results. We use a value of $Da = 2 \times 10^4$ to approximate an infinite Damköhler number in all calculations unless otherwise specified.

We begin with an illustrative calculation, shown in figure 10, which displays the nature of the instability that occurs if Ra takes a value slightly higher than Ra_c. The figure shows the stationary, stable states that the system reaches for two selected values of S when $Ra > Ra_c$. The mechanism of the fluid instability is similar to that of the non-reactive case, described in detail by Chandrasekhar (1961, pp. 9–10) and Getling (1998, p. 12), whereby fluid of higher density lies above the hotter, lower-density fluid causing convection to occur. The induced flow enhances the transport of fuel and oxidizer to certain parts of the flame, generating a cellular structure, as shown in the figure.

Next, we test the validity of the linear stability results in the Boussinesq approximation and the effect of compressibility on the critical Rayleigh number. In figure 11 we plot the relationship between (*a*) $Ra_{c,scaled}$ and S and (*b*) $Ra_{c,scaled}$ and y_{st} for several values of the thermal expansion coefficient α. We also plot $Ra_{c,scaled}$ as

https://doi.org/10.1017/jfm.2013.549 Published online by Cambridge University Press

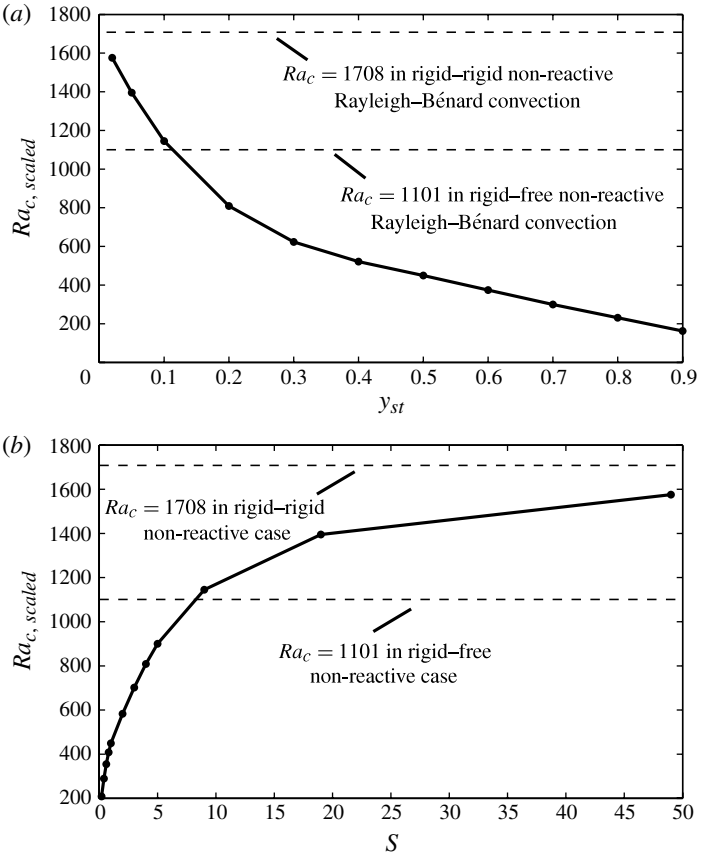


FIGURE 9. The effect of (*a*) the flame position $y_{st} = 1/(1 + S)$ and (*b*) the stoichiometric coefficient S on the scaled critical Rayleigh number $Ra_{c,scaled}$. Indicated are the critical Rayleigh numbers in non-reactive Rayleigh–Bénard convection with two rigid boundaries and with one rigid boundary and one free boundary.

predicted by the linear stability analysis, for comparison. As expected, the values of $Ra_{c,scaled}$ calculated for a low value of α are similar to the values calculated in the linear stability analysis. This is because the Boussinesq approximation is derived from an expansion in small α of the governing equations.

The numerical results corresponding to larger, more realistic values of the thermal expansion coefficient show several discrepancies with those of the linear stability analysis. First, the non-Boussinesq system is found to be more stable, a well-known result in non-reactive Rayleigh–Bénard convection (see Bormann 2001). Secondly, the system is found to exhibit hysteresis at the onset of instability, whereby the system allows two different steady states for the same parameter values as shown in figure 12; again, it is well-known in the literature for the non-reactive case that this is associated with departures from the Boussinesq approximation (see Fröhlich *et al.* 1992; Getling 1998, p. 23). Despite these differences, figure 11(*b*) shows that the relationship between Ra_c and S is found to be qualitatively similar for all of the selected values of α.

https://doi.org/10.1017/jfm.2013.549 Published online by Cambridge University Press

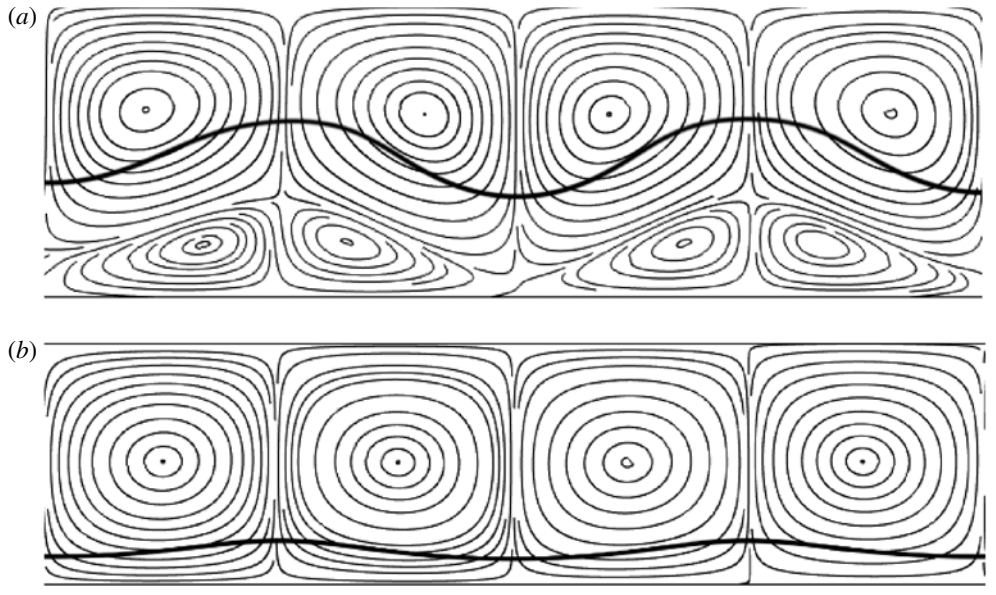


FIGURE 10. Convection roll/cellular flame steady-state streamlines for different values of the stoichiometric coefficient S in the Boussinesq approximation: (*a*) $S = 1$, computed at $Ra = 3700$; (*b*) $S = 6$, computed at $Ra = 1740$. The black line represents the flame position. Calculations were performed with the parameter values $Da = 2 \times 10^4$, $\beta = 10$ and $Pr = 1$ and for values of the Rayleigh number Ra slightly higher than its critical value Ra_c in each case.

To close this section, we now test the effect of finite chemistry on the critical Rayleigh number by varying the Damköhler number Da. The results, presented in figure 13, show that Ra_c decreases as Da decreases. In the limit $Da \to \infty$ there is little change in Ra_c as Da varies; indeed, the curve in the figure can be seen to flatten out near $Da = 1000$. Thus the value $Da = 2 \times 10^4$ used previously to approximate infinitely fast chemistry is sufficiently large. As Da approaches its extinction value Da_{ext} the system becomes considerably more unstable and Ra_c is reduced significantly.

8. Conclusion

We have studied, using analytical and numerical methods, the stability of a planar diffusion flame in an infinitely long porous channel under gravitational effects. The conditions under which the diffusion flame becomes unstable have been determined by calculation of the critical Rayleigh number, which defines the threshold of instability. Such results do not seem to be available in the literature.

First, we have investigated the stability of the Burke–Schumann flame, using a linear stability analysis in the Boussinesq approximation. The relationship between the position of the flame in the channel (governed by the stoichiometric coefficient) and the critical Rayleigh number has been determined. The growth rate of the linear stability problem was first confirmed to be real using numerical methods, so that the system could be studied analytically in the marginal state using a similar method to that of the non-reactive problem.

Results have been presented, which show that as the flame approaches the lower boundary with increasing stoichiometric coefficient, the critical Rayleigh number is

https://doi.org/10.1017/jfm.2013.549 Published online by Cambridge University Press

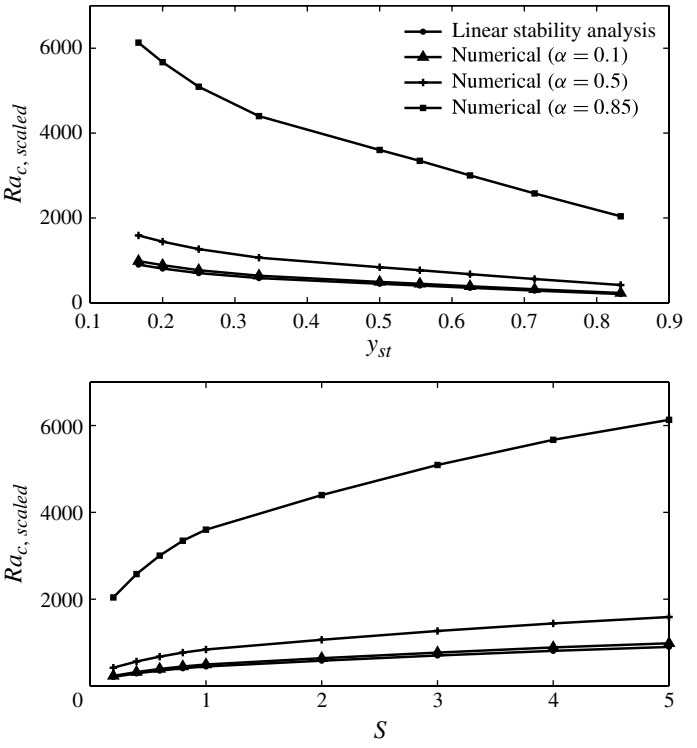


FIGURE 11. Comparison of the behaviours of the scaled critical Rayleigh numbers $Ra_{c,scaled}$ versus (*a*) flame position $y_{st} = 1/(1 + S)$ and (*b*) stoichiometric coefficient S as predicted by the linear stability analysis and the computations carried out for selected values of the thermal expansion coefficient α. Numerical calculations were performed for the parameter values $Da = 2 \times 10^4$, $\beta = 10$ and $Pr = 1$.

close to the well-known value it takes in the non-reactive case with two rigid boundaries. A rescaling of the Rayleigh number using the distance between the flame and the cold upper boundary as reference length was performed to aid in the comparison between the reactive and non-reactive problems. The scaled critical Rayleigh number was found to be (*a*) of the order of magnitude of the critical Rayleigh number in the non-reactive problem with two rigid boundaries, as the flame approaches the lower wall and (*b*) of the order of magnitude of the critical Rayleigh number in the non-reactive problem with one rigid and one free-surface boundary, when the flame is located a certain distance from the lower wall (which has been calculated).

Secondly, we have performed numerical calculations in the low-Mach-number formulation for several values of the thermal expansion coefficient using a finite-element method with a high Damköhler number. The results show that when the Rayleigh number is higher than its critical value, the fluid forms convection rolls as in the non-reactive case, which interact with the flame to generate cellular structures.

For weak values of the thermal expansion coefficient α, which corresponds to conditions for which the Boussinesq approximation is valid, the numerical results show strong agreement with those of the linear stability analysis. For larger values of α, there is qualitative agreement between the numerical and analytical results but several

https://doi.org/10.1017/jfm.2013.549 Published online by Cambridge University Press

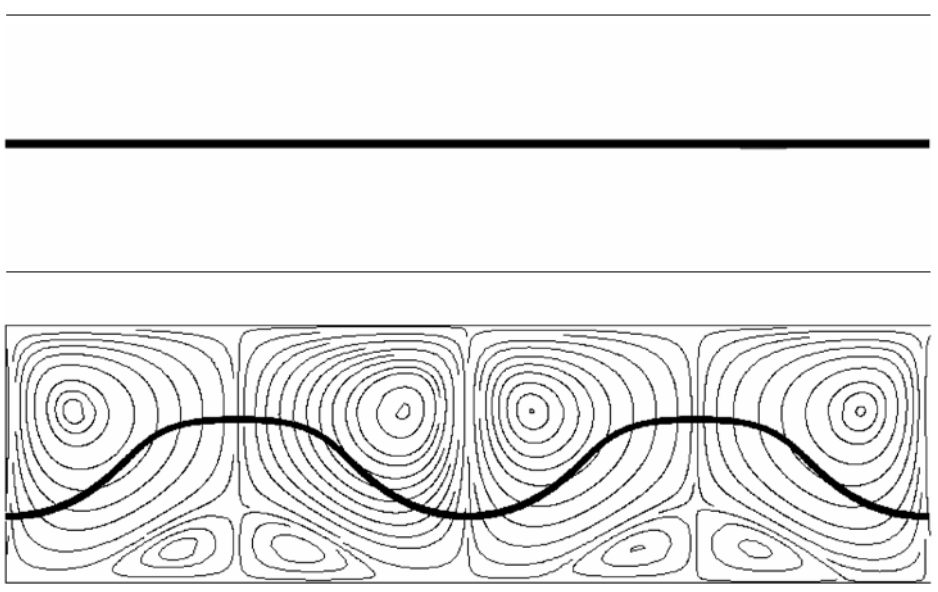


FIGURE 12. Numerical calculations displaying an example of hysteresis in the non-Boussinesq system: (*a*) strongly burning planar diffusion flame with no flow (quiescent state); (*b*) convection roll/cellular flame state with streamlines. The black line represents the flame position. Both calculations were performed for the parameter values $\alpha = 0.85$, $Da = 2 \times 10^4$, $S = 1$, $\beta = 10$, $Pr = 1$ and for $Ra = 28\,000$, which is lower than Ra_c for these parameter values. Both steady states are found to be stable, and since they both exist for $Ra < Ra_c$, this is an example of a finite-amplitude subcritical instability of the quiescent state.

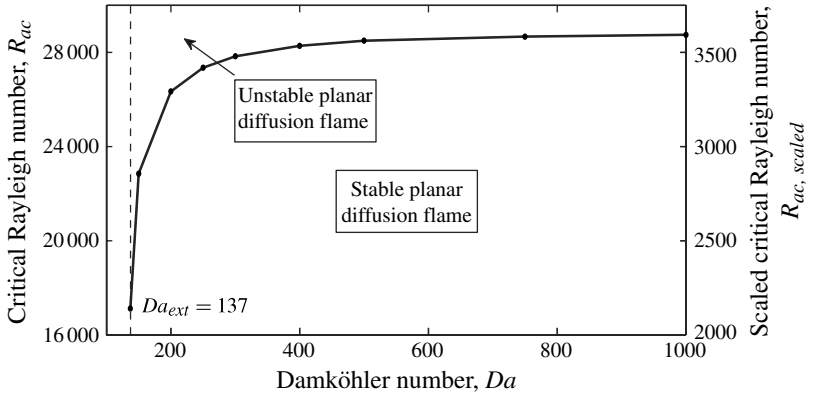


FIGURE 13. The effect of the Damköhler number Da on the critical Rayleigh number Ra_c and the scaled critical Rayleigh number $Ra_{c,scaled}$. The calculations were performed for the parameter values $\alpha = 0.85$, $\beta = 10$, $S = 1$ and $Pr = 1$. Indicated in the figure is the extinction value of Da, below which the strongly burning planar diffusion flame cannot exist.

discrepancies caused by a higher thermal expansion coefficient. The non-Boussinesq system was found to be more stable than the system in the Boussinesq approximation

https://doi.org/10.1017/jfm.2013.549 Published online by Cambridge University Press

and to exhibit hysteresis at the onset of instability, which are well-known results in the non-reactive case.

Finally, we have investigated the effect of finite chemistry on the system. The results show that the system becomes less stable as the Damköhler number Da is decreased, especially as Da approaches its extinction value Da_{ext}, below which the strongly burning diffusion flame cannot exist. For large values of Da the decrease in the critical Rayleigh number with decreasing Da was found to be small.

The results in this paper are a crucial step in the understanding of gravitational effects on diffusion flames with important ramifications for combustion in non-uniform mixtures such as triple flames. Further studies will concentrate on the effect of gravity on the stability of triple flames, and will be helped by the characterization of the instability of their trailing planar diffusion flame studied in this paper.

REFERENCES

AHLERS, G., GROSSMANN, S. & LOHSE, D. 2009 Heat transfer and large-scale dynamics in turbulent Rayleigh–Bénard convection. *Rev. Mod. Phys.* **81** (2), 503–537.

ARAI, M., SATO, H. & AMAGAI, K. 1999 Gravity effects on stability and flickering motion of diffusion flames. *Combust. Flame* **118** (1), 293–300.

BÉNARD, H. 1900 Les tourbillons cellulaires dans une nappe liquide. *Rev. Gen. Sci. Pures Appl.* **11** (1309), 1261–1271.

BODENSCHATZ, E., PESCH, W. & AHLERS, G. 2000 Recent developments in Rayleigh–Bénard convection. *Annu. Rev. Fluid Mech.* **32** (1), 709–778.

BORMANN, A. S. 2001 The onset of convection in the Rayleigh–Bénard problem for compressible fluids. *Contin. Mech. Thermodyn.* **13** (1), 9–23.

BOUSSINESQ, J. 1903 *Theorie Analytique de la Chaleur*. Gauthier-Villars.

BUCKMASTER, J. & JACKSON, T. L. 2000 Holes in flames, flame isolas, and flame edges. *Proc. Combust. Inst.* **28** (2), 1957–1964.

BUCKMASTER, J. D. & LUDFORD, G. S. S. 1983 *Lectures on Mathematical Combustion*. SIAM.

BUCKMASTER, J., NACHMAN, A. & TALIAFERRO, S. 1983 The fast-time instability of diffusion flames. *Physica* D **9** (3), 408–424.

BUCKMASTER, J. & PETERS, N. 1988 The infinite candle and its stability – A paradigm for flickering diffusion flames. *Symp. (Intl) Combust.* **21** (1), 1829–1836.

BYCHKOV, V., MODESTOV, M., AKKERMAN, V. & ERIKSSON, L. E. 2007 The Rayleigh–Taylor instability in inertial fusion, astrophysical plasma and flames. *Plasma Phys. Control. Fusion* **49** (12B), B513.

CHANDRASEKHAR, S. 1961 *Hydrodynamic and Hydromagnetic Instability*. Dover.

CHEATHAM, S. & MATALON, M. 1996*a* Heat loss and Lewis number effects on the onset of oscillations in diffusion flames. In *Symp. (Intl) Combust.*, 26, pp. 1063–1070.

CHEATHAM, S. & MATALON, M. 1996*b* Near-limit oscillations of spherical diffusion flames. *AIAA J.* **34** (7), 1403–1409.

CHEATHAM, S. & MATALON, M. 2000 A general asymptotic theory of diffusion flames with application to cellular instability. *J. Fluid Mech.* **414**, 105–144.

DAOU, J. & AL-MALKI, F. 2010 Triple-flame propagation in a parallel flow: an analytical study. *Combust. Theor. Model.* **14** (2), 177–202.

ECHEKKI, T., CHEN, J. Y. & HEGDE, U. 2004 Numerical investigation of buoyancy effects on triple flame stability. *Combust. Sci. Technol.* **176** (3), 381–407.

FRÖHLICH, J., LAURE, P. & PEYRET, R. 1992 Large departures from Boussinesq approximation in the Rayleigh–Bénard problem. *Phys. Fluids* A **4**, 1355.

GELFGAT, A. Y. 1999 Different modes of Rayleigh–Bénard instability in two- and three-dimensional rectangular enclosures. *J. Comput. Phys.* **156** (2), 300–324.

GETLING, A. V. 1998 *Rayleigh–Bénard Convection: Structures and Dynamics*. World Scientific.

https://doi.org/10.1017/jfm.2013.549 Published online by Cambridge University Press

JIANG, X. & LUO, K. H. 2000 Combustion-induced buoyancy effects of an axisymmetric reactive plume. *Proc. Combust. Inst.* **28** (2), 1989–1995.

KIM, J. S. 1997 Linear analysis of diffusional-thermal instability in diffusion flames with Lewis numbers close to unity. *Combust. Theor. Model.* **1** (1), 13–40.

KIM, J. S., WILLIAMS, F. A. & RONNEY, P. D. 1996 Diffusional-thermal instability of diffusion flames. *J. Fluid Mech.* **327**, 273–301.

KIRKBEY, L. L. & SCHMITZ, R. A. 1966 An analytical study of the stability of a laminar diffusion flame. *Combust. Flame* **10** (3), 205–220.

KUKUCK, S. & MATALON, M. 2001 The onset of oscillations in diffusion flames. *Combust. Theor. Model.* **5** (2), 217–240.

LIÑÁN, A. 1974 The asymptotic structure of counterflow diffusion flames for large activation energies. *Acta Astronaut.* **1** (7), 1007–1039.

LOHSE, D. & XIA, K. Q. 2010 Small-scale properties of turbulent Rayleigh–Bénard convection. *Annu. Rev. Fluid Mech.* **42**, 335–364.

MAJDA, A. & SETHIAN, J. 1985 The derivation and numerical solution of the equations for zero Mach number combustion. *Combust. Sci. Technol.* **42** (3–4), 185–205.

MATALON, M. 2009 Flame dynamics. *Proc. Combust. Inst.* **32** (1), 57–82.

MATALON, M. & METZENER, P. 2010 The effect of thermal expansion on diffusion flame instabilities. *J. Fluid Mech.* **647**, 453–472.

MATKOWSKY, B. J. & SIVASHINSKY, G. I. 1979 An asymptotic derivation of two models in flame theory associated with the constant density approximation. *SIAM J. Appl. Maths* **37** (3), 686–699.

METZENER, P. & MATALON, M. 2006 Diffusive-thermal instabilities of diffusion flames: onset of cells and oscillations. *Combust. Theor. Model.* **10** (4), 701–725.

MIKLAVČIČ, M., MOORE, A. B. & WICHMAN, I. S. 2005 Oscillations and island evolution in radiating diffusion flames. *Combust. Theor. Model.* **9** (3), 403–416.

PAILLERE, H., VIOZAT, C., KUMBARO, A. & TOUMI, I. 2000 Comparison of low Mach number models for natural convection problems. *Heat Mass Transfer* **36** (6), 567–573.

RAYLEIGH, LORD 1916 On convection currents in a horizontal layer of fluid, when the higher temperature is on the under side. *Phil. Mag.* **32** (192), 529–546.

REHM, R. G. & BAUM, H. R. 1978 The equations of motion for thermally driven, buoyant flows. *J. Res. Natl Bur. Stand.* **83** (3), 297–308.

SHAMPINE, L. F., KIERZENKA, J. & REICHELT, M. W. 2000 Solving boundary value problems for ordinary differential equations in MATLAB with bvp4c. *Tech Rep*. The MathWorks.

SIVASHINSKY, G. I. 1977 Nonlinear analysis of hydrodynamic instability in laminar flames – i. Derivation of basic equations. *Acta Astronaut.* **4** (11), 1177–1206.

SOHN, C. H., CHUNG, S. H. & KIM, J. S. 1999 Instability-induced extinction of diffusion flames established in the stagnant mixing layer. *Combust. Flame* **117** (1), 404–412.

VANCE, R., MIKLAVCIC, M. & WICHMAN, I. S. 2001 On the stability of one-dimensional diffusion flames established between plane, parallel, porous walls. *Combust. Theor. Model.* **5** (2), 147–161.

WU, K. K. & CHEN, C. H. 2003 A numerical analysis of ignition to steady downward flame spread over a thin solid fuel. *Combust. Sci. Technol.* **175** (5), 933–964.

https://doi.org/10.1017/jfm.2013.549 Published online by Cambridge University Press